Brigham Young University
BYU ScholarsArchive

All Theses and Dissertations

2017-03-01

An Analytical Model to Predict the Length of Oxygen-Assisted, Swirled, Coal and Biomass Flames

David Arthur Ashworth
Brigham Young University

Follow this and additional works at: https://scholarsarchive.byu.edu/etd

 Part of the Mechanical Engineering Commons

BYU ScholarsArchive Citation

Ashworth, David Arthur, "An Analytical Model to Predict the Length of Oxygen-Assisted, Swirled, Coal and Biomass Flames" (2017). *All Theses and Dissertations*. 6286.
https://scholarsarchive.byu.edu/etd/6286

This Thesis is brought to you for free and open access by BYU ScholarsArchive. It has been accepted for inclusion in All Theses and Dissertations by an authorized administrator of BYU ScholarsArchive. For more information, please contact scholarsarchive@byu.edu, ellen_amatangelo@byu.edu.

An Analytical Model to Predict the Length of Oxygen-Assisted, Swirled, Coal and Biomass Flames

David Arthur Ashworth

A thesis submitted to the faculty of
Brigham Young University
in partial fulfillment of the requirements for the degree of

Master of Science

Dale R. Tree, Chair
Julie Crockett
David O. Lignell

Department of Mechanical Engineering

Brigham Young University

Copyright © 2017 David Arthur Ashworth

All Rights Reserved

ABSTRACT

An Analytical Model to Predict the Length of Oxygen-Assisted, Swirled, Coal and Biomass Flames

David Arthur Ashworth
Department of Mechanical Engineering, BYU
Master of Science

Government regulations to reduce pollutants and increasing environmental awareness in the power generation industry have encouraged coal power plants to begin firing biomass in their boilers. Biomass generally consists of larger particles which produce longer flames than coal for a given burner. The length of the flame is important in fixed-volume boilers because of its influence on heat transfer, corrosion, deposition, and pollutant formation.

Many pulverized fuel burners employ a series of co-annular tubes with various flows of fuel and air to produce a stabilized flame. A variable swirl burner with three co-annular tubes, each of variable diameter, has been used to collect flame length data for nearly 400 different operating conditions of varying swirl, fuel type, air flow rate, enhanced oxygen flow rate and oxygen addition location. A model based on the length required to mix fuel and air to a stoichiometric mixture was developed.

Inputs to the model are the flow rates of fuel, air, and oxygen, swirl vane position and burner geometries. The model was exercised by changing flow rates and burner tube diameters one at a time while holding all others constant. Physical explanations for trends produced were given.

The model also requires two constants, one of which is solved for given a case without swirl, and the other is found by fitting experimental data. The constants found in this study appear to be accurate exclusive to the BYU burner. Thus burner designers will need to obtain minimal amounts of data to predict constants for their reactor and then employ the model to predict flame length trends.

The resulting correlation predicts 90% of the flame lengths to be within 20% of the measured value. The correlation provides insights into the expected impact of burner flow rates and geometry changes on flame length which impacts particle burnout, NOx formation and heat transfer.

Keywords: flame length, coal, biomass, oxygen assisted, pulverized fuel, combustion model

ACKNOWLEDGEMENTS

I am very grateful for the education and experience I have gained as a graduate student at Brigham Young University. My interactions with fellow students, faculty, and staff have all contributed to my academic success.

I would like to firstly thank Dr. Tree for constant mentoring and hours spent giving me careful attention and instruction for my personal development and growth. I would like to thank my colleagues, John Tobiasson, Nathan Day, Steven Owen, and Daniel Ellis in the combustion lab for their technical support and good examples. I would like to also thank my family, especially my wife Sherrie for her support of my educational goals and the care she provided for our three children at home while I spent countless hours and many late nights on campus.

Finally I would like to thank Air Liquide for the funding that made this work possible, particularly Bhupesh and his colleagues for their communication and in-person visits.

TABLE OF CONTENTS

LIST OF TABLES

LIST OF FIGURES

NOMENCLATURE

Abbreviations

ASTM	American Society for Testing and Materials
BFR	Burner Flow Reactor
BYU	Brigham Young University
C	Carbon
CFD	Computational fluid dynamics
CO	Carbon Monoxide
CO_2	Carbon Dioxide
CPD	Coal Percolation and Devolatilization
°C	Degrees Celsius
EPA	Environmental Protection Agency
HCN	Hydrogen Cyanide
HHV	Higher Heating Value
kg/hr	Kilograms Per Hour
kW_{th}	Kilowatts of Thermal Power
K	Kelvin
LOI	Loss on Ignition
m	Meters
mm	Millimeters
N_2/N	Nitrogen
NO	Nitric Oxide
NO_2	Nitrogen Dioxide
NO_x	Nitrogen Oxides
O_2/O	Oxygen
ppm	Parts Per Million
µm	Microns or Micrometers
wt %	Weight Percent
W_{mfa}	Weight of Ash with Moisture Removed
W_{cfa}	Weight of Carbon Free Ash
Y_{ash}	Mass Fraction of Ash

Latin Symbols

b	Theoretical diameter of recirculation zone
c_1	Proportionality constant for shearing term
c_2	Empirical constant for swirl term
c_s	Stoichiometric mixture of fuel to oxidizer
d_c	Diameter of center tube
d_p	Diameter of primary tube
L_f	Flame length
$\dot{m}_{fuel}$	Total mass flow of solid fuel
$\dot{m}_{ox}$	Total mass flow of oxidizer
$\dot{m}_{O_2,p}$	Mass flow of oxygen in primary flow
$\dot{m}_{O_2,c}$	Mass flow of oxygen in center tube
ρ_{mix}	Density of fuel-air mixture in primary flow
ρ_{sec}	Density of air in secondary flow
S	Swirl number
U_{RZ}	Tangential velocity of secondary flow induced by swirl
V_p	Velocity of primary flow
V_{sec}	Velocity of secondary flow
$Y_{fuel,p}$	Mass fraction of fuel in primary flow
$Y_{O_2,sec}$	Mass fraction of oxygen in secondary flow

1 INTRODUCTION

Energy efficiency and pollutant emissions will always be a major topic of discussion among scientists and politicians. Pollutants have negative impacts on the environment, global climate change, and human health. Among the most hazardous atmospheric pollutants, nitrogen oxides (NO and NO_2, or NOx) are well known for their poisonous and smog-promoting properties. Power plant boilers produce 40% of the NO_x emissions from stationary sources [1]. Recent regulations in the United States, such as the Clean Air Act [2] and its amendments, have been created to ensure cleaner and more efficient energy production. In order to meet new regulations much effort has been invested into technologies that may reduce NO_x in solid, pulverized fuel-fired boilers. Burner design alone has been shown to significantly reduce NOx emissions, as well as improve particle burnout [3]. Low NO_x burners are one example of an emerging burner design of recent decades specifically intended to reduce NO_x in boilers [4]. However, optimizing these designs can be quite complex, requiring significant amounts of time and money invested into modeling the process. Computational fluid dynamics (CFD) is frequently used but requires massive amounts of data processing which becomes very expensive. Inexpensive and less time intensive models could be beneficial for preliminary design stages of new burner configurations and for optimal operation of existing burners.

Cofiring biomass with coal is currently a popular option for CO_2 reduction. However, biomass is not pulverized as easily as coal, and larger biomass particles can create longer volatile

flames [5]. Owen et. al. [3] demonstrated that longer biomass flames tend to reduce NO_x formation, but also reduce particle burnout. Flame length also affects the dynamics in boilers including heat transfer, deposition, and corrosion. Altering the fuel composition will change the flame length, which is problematic for expensive coal boilers originally designed to burn coal. Rebuilding entire boilers can be financially impractical, but altering burner operation or redesigning the burners is much more feasible. One option for improved burner operation is the selective addition of oxygen at various locations and in various flow streams. Another is the change of burner dimensions and flow rates. To assist the designing of new burners a large set of empirical data were collected and evaluated relative to NO, LOI, and flame length. A model explaining trends in the data and correlating trends in flame length as a function of burner parameters is sought. This work presents such a correlation and provides explanations of the trends it produces.

1.1 Objectives

The objective of this work is to collect additional flame length data from a wider range of fuels including switchgrass and coal and to use these data to evaluate and refine the flame length model originally proposed by Owen et. al. [3]. Visual flame length data will be collected in BYU's burner flow reactor and compared to the model's predicted values for five solid fuels including various types of biomass and coal. The model is then exercised to show various trends produced by changing specific burner and flow parameters. NO_x and burnout data will also be examined to illustrate the importance of predicting flame length.

1.2 Scope

This work will demonstrate how certain design parameters affect volatile flame length for solid pulverized fuel combustion. Flame length is measured visually and predicted analytically. Empirical constants in the model will be derived by error minimization for each fuel. Two fuels; coal and switchgrass will be added to the existing data set of straw, medium wood and fine wood previously collected. Measurements will include visual flame length, exhaust NO, CO, CO_2 and O_2 concentration and cyclone collection of ash for LOI analysis. No comprehensive combustion analysis or CFD is included in this work.

2 LITERATURE REVIEW

This chapter provides a review of previous methods used to predict flame length categorized by flame type. In the descriptions which follow below, models have been developed for various types of flames that determine the location of a stoichiometric mixture. This location is then compared to some type of flame length measurement.

2.1 Laminar Diffusion Flames

Laminar diffusion flames have been probed and modeled extensively for decades because of the relative simplicity of their geometry and flow and yet a mathematical description of even the simplest flame and geometry is challenging because of the necessity to describe mass, energy, momentum, and chemical reactions simultaneously.

Burke and Schumann [6] provided some of the earliest mathematical descriptions of cylindrical laminar flames. They presented a method to calculate flame length for a circular port gas burner with co-flowing air. Their model is used to find the length at which the stoichiometric ratio of fuel and oxygen occurs along the axis of the flame. In their model they assumed that the axial gas velocity was constant throughout the fuel and surrounding oxidizer thus producing mixing only by diffusion. The diffusion coefficient of the gas and air is constant. Their model, confirmed by experimental data, showed that flame length is related to the burner diameter,

diffusion coefficient, viscosity, and stoichiometric fuel air ratio but the relationships between these variables are not easily determined from their result.

Roper [7] observed that while Burke and Schumann's model was accurate for circular port burners, it was not accurate for burners of other geometries. Roper still assumed a constant velocity profile across the radial axis of the flame but modified the assumption by allowing velocity to change in the axial direction to include acceleration due to buoyancy. Equations were then derived for flame height for a circular or square port burner and for slot burners controlled by momentum or buoyancy, or both by superposition. Roper's [7] results show that flame length is proportional to volume flow rate and inversely proportional to the diffusion coefficient and stoichiometric fuel mass fraction in addition to burner geometry relationships. For a given fuel and ambient conditions, the common factor affecting flame height for each type of flame/burner is the volumetric flow rate of fuel.

The work of Burke and Schumann [6] and that of Roper [7, 8] are reviewed by Turns [9] who utilizes the mixture fraction as a scalar quantity in the mass transport equation and develops fundamental mass, energy, species, and momentum equations for a reacting circular jet. Solving these equations for the centerline location ($r = 0$) where the mixture is stoichiometric identifies the flame length. The result is shown in Equation 2.1 where Q_F is the volumetric flow rate of gaseous fuel, $\mathcal{D}$ is a diffusion coefficient, and $Y_{F,stoic}$ is the stoichiometric mass fraction of fuel. This indicates that for a given gaseous fuel, flame length is only a function of the volumetric flow rate of the fuel.

$$L_f \approx \frac{3}{8\pi}\frac{1}{\mathcal{D}}\frac{Q_F}{Y_{F,stoic}} \tag{2.1}$$

This equation indicates that if a laminar burner diameter where doubled, the flame length would remain unchanged because the increased time required to diffuse oxidizer to the center of the flame would be offset by the increased time for the flow to reach a particular length from the burner.

Turns proceeds to reference work done by Fay [10] in which density is no longer assumed to be constant. In this case, the variable-density solution is given by Equation 2.2 wherein flame length is still a function of the volume flow rate as before but is also a function of the fuel and ambient densities.

$$L_f \approx \frac{3}{8\pi}\frac{1}{Y_{F,stoic}}\frac{Q_F}{\mathcal{D}_{ref}}\frac{\rho_F\rho_\infty}{{\rho_{ref}}^2}\frac{1}{I\left(\rho_\infty/\rho_f\right)} \tag{2.2}$$

The modeling results of Burke and Schumann [6] and Turns [9] ignore the effects of buoyancy and yet the results tend to match experimental data fairly well. This is because while buoyancy tends to accelerate the flow increasing the effective volume flow rate Q_F which would tend to increase flame length, it also increases the velocity gradient between the fuel and oxidizer and therefore increases mixing above the pure diffusion assumed in Equation 2.2 which tends to decrease flame length. Thus, the two effects tend to offset each other for diffusion flames and the results of Burke and Schumann [6] and Turns [9] are relatively accurate. Laminar diffusion flames are therefore readily correlated by volume flow rate, fuel stoichiometric mass fraction, and the diffusion coefficient.

2.2 Turbulent Flames

Although laminar diffusion flames are relatively simple and more easily modeled, turbulent flames are used much more frequently in industrial applications. Turbulence has important flow and mixing effects which add a significant amount of complexity to modeling.

Shearing between flows can no longer be neglected, i.e. the assumption of a constant velocity profile is invalid, and the enhanced mixing of turbulent eddies becomes important.

Due to the extreme complexity and apparent randomness of turbulence, analytical models are often developed through correlations based on experimental data. Turns [11] reviewed the work of Wohl et al. [12] in 1949 who found that while laminar flames are a function of volumetric flow rate and independent of initial jet diameter, this is not the case for turbulent flames. Beyond the laminar-turbulent transition regime, increasing flowrate does not affect flame length significantly, and the degree to which it affects flame length appears to be dependent on burner diameter. In fact, for smaller burner diameters flame length remains nearly constant. This occurs because as flowrate increases, mixing and air entrainment also increases nearly proportional to flowrate, which shortens the flame and counteracts the lengthening effect of higher flowrates.

In 1993, Delichatsios [13] performed a study based on work by Becker and Liang [14] (1978) on the entire range of turbulent vertical flames, from pool fires (buoyancy-driven or natural convection) to jet flames (momentum-driven or forced convection). This study correlated visible flame length data with the Froude number of flow. He then developed a "flame Froude number" for jet flames which includes effects of combustion stoichiometry. From equations developed by Delichatsios, Turns [11] outlines a simple approach to analytically solve for the flame length of a fuel jet issuing from a nozzle of diameter, d_j, into ambient air conditions (∞) as shown in Equations 2.3 through 2.5 where Fr_f is the flame Froude number, v_e is the fuel nozzle exit velocity, f_s is stoichiometric mixture fraction, ρ_e is the fuel density, ΔT_f is the characteristic temperature rise from combustion, and L^* is a dimensionless flame length.

$$Fr_f = \frac{v_e f_s^{3/2}}{\left(\frac{\rho_e}{\rho_\infty}\right)^{1/4}\left(\frac{\Delta T_f}{T_\infty} g d_j\right)^{1/2}} \tag{2.3}$$

$$L^* = \frac{13.5 Fr_f^{2/5}}{\left(1 + 0.07 Fr_f^2\right)^{1/5}} \tag{2.4}$$

$$L_f = \frac{L^* d_j \sqrt{\rho_e/\rho_\infty}}{f_s} \tag{2.5}$$

This model shows us that the four primary factors that affect flame length of turbulent jets are: 1) the relative influence of momentum and buoyancy (Fr_f), 2) stoichiometric mixture fraction (f_s), 3) fuel to air density ratio (ρ_e/ρ_∞), and 4) jet diameter (d_j). At large flame Froude numbers ($Fr_f >> 1$) or flames which have strong initial jet momentum, the flame length is independent of the Fr_f, and is only dependent on the burner jet diameter (d_j) and fuel stoichiometric mixture fraction, or for a given fuel the flame length is dependent only on the burner diameter.

Much of the work on turbulent diffusion flames was comprehensively outlined in a recent publication on predicting the geometry (length, width, and volume) of laminar, turbulent, and transition jet diffusion flames by Kang et al. [15]. Like most other combustion models conservation of mass and momentum equations are employed with various assumptions made for each type of flame.

2.3 Swirled Turbulent Flames

Turbulent flames are often stabilized by adding swirled air around the fuel. Experiments have shown that swirl also creates shortened, intense flames [16]. As with laminar and turbulent

jet flames, the flame length can be calculated by the distance required to entrain enough oxidizer to create a stoichiometric mixture.

Figure 2.1 shows a schematic diagram of the air and fuel flow velocities of a simple swirled jet burner. The air is given a tangential velocity which creates a recirculation zone after exiting the burner. Chen and Driscoll [17] point out that there are two sources of oxidizer penetration into the fuel rich region. One is by laminar or turbulent diffusion at the boundary of the fuel and oxidizer jet as is found in laminar and jet diffusion flames. The second is the entrainment of recirculated oxidizer as shown in Figure 2.1. Recirculating flow at the end of the recirculation zone travels back toward the burner exit along the axial length of the recirculation zone. Mixing occurs radially along the axial streams of recirculating oxidizer

The volumetric stoichiometric fuel/air mixture ratio can be created as shown in Equation 2.6 where the numerator is the volumetric flow of fuel exiting the primary fuel tube of diameter d_F at velocity U_F, while the numerator is the volume flow rate of the oxidizer mixing into the fuel stream quantified by a cylindrical volume defined by πbL and a characteristic mixing velocity U_c, where L is the flame length, and b is the widest diameter where the average axial velocity is zero. Thus, the mixing of oxidizer is approximated to occur along a cylindrical boundary of diameter, b, and length, L.

$$C_s = \frac{\frac{\pi {d_F}^2}{4} U_F}{\pi b L U_C} \tag{2.6}$$

This characteristic mixing velocity is argued to be the sum of two components as shown in Equation 2.7. The first is due to recirculation while the second is due to shearing between the fuel and air streams.

$$U_C = \pi b L U_{RZ} + \pi L |U_F - U_A| d_F Const \tag{2.7}$$

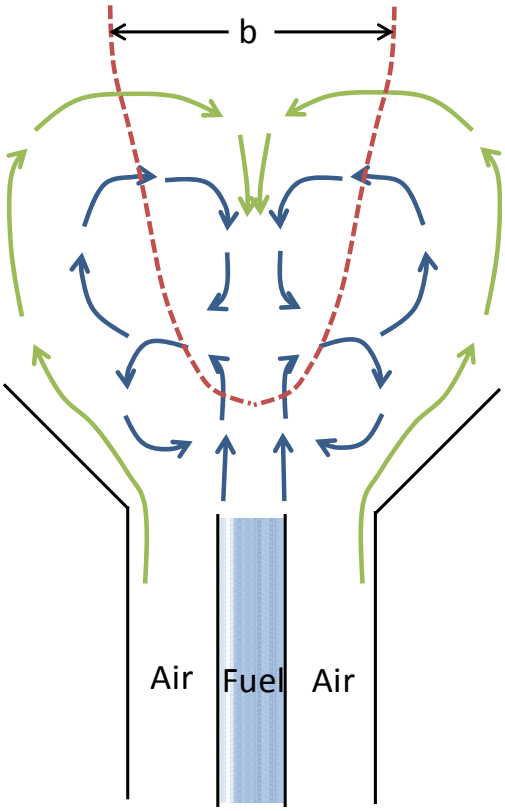

Figure 2.1: Schematic diagram of the fuel and air flow of a simple swirled gas flame

To quantify the strength of such a recirculation zone, a characteristic recirculation zone velocity, U_{RZ} was be defined by Equation 2.8 where U_Z is the mean axial velocity and b is the radial location where U_Z becomes zero, i.e. the boundary of the recirculation zone where flow has turned to be perpendicular to the jet axis.

$$U_{RZ} = \int_0^b -U_Z 2\pi r \, dr / \pi b^2 \tag{2.8}$$

Chen and Driscoll measured U_{RZ} and b using laser Doppler velocimetry and compared them to the swirl number defined as the ratio of angular momentum flux to axial momentum flux. They found that both U_{RZ} and b increased up until a swirl number of about 0.5, at which point they believed shear stresses prevented further increase. Substituting Equation 2.7 into

Equation 2.6 can yield Equation 2.9 where L is flame length, subscript A denotes values for the air stream and subscript F denotes values for the fuel stream, U is velocity, d is diameter, and $\dot{m}$ is mass flow, and c_1 and c_2 are empirically derived proportionality constants.

$$\frac{L}{d_A} = \frac{c_1(\dot{m}_F/\dot{m}_A)}{\left(\frac{U_{RZ}b}{U_A d_A} + \frac{|U_A - U_F|}{U_A}\frac{d_F}{d_A}c_2\right)} \tag{2.9}$$

In general the numerator accounts for stoichiometry and in the denominator, the U_{RZ} term describes the mixing effects of swirl on flame length and the $|U_A - U_F|$ term describes the viscous shear mixing effects between streams. This model shows that the primary factors that affect flame length are stoichiometry, swirl, viscous shearing, and burner geometry and that a relatively simple model can successful predict the length of swirled, turbulent gaseous flames.

2.4 Pulverized Solid Fuel Models

The complexity of flame length models increases dramatically when the fuel becomes a flow of pulverized, solid particles rather than a gas. The fuel is no longer burning in only a homogenous (gas-gas) reaction but also in heterogeneous (solid-gas) reactions. Particle heating, devolatilization and char oxidation are complex processes of which many researchers have attempted to obtain good experimental data and produce models to predict various reaction rates [18, 19]. The molecular structure of coal, not to mention other solid fuels such as biomass, varies widely and is not even thoroughly understood yet [20]. Turns [21] provides a good, surface-level overview of several other challenges of modeling solid fuel flames. In order to capture all of these effects, CFD models have frequently been used to generate the length of solid fuel flames which take into account both the complex decomposition of individual particles, including devolatilization and char oxidation, as well as flow characteristics, such as turbulence [22, 23].

One recent study demonstrated much of the complexity involved in attempting to predict flame length in solid fuel combustion. Holtmeyer et al. [5] used CFD to model co-fired flames of pulverized coal and wood waste. Flame length was defined by the point at which CO concentration was within 15% of its asymptotic value along the axial length of the combustion chamber. It was discussed that because biomass has a much larger volatile fraction, cofiring with coal should create longer volatile flames than coal alone. However data showed just the opposite for biomass cofiring rates below 30%. It was concluded that the most likely cause was larger biomass particles not releasing volatiles until after passing beyond the coal volatile reaction zone where the volatiles from coal and smaller wood particles react. This reduces the amount of gaseous fuel reacting near the burner and thus a shorter volatile flame length. Cofiring rates beyond 30% appeared to lengthen the flame linearly as larger wood particles began to dominate combustion behavior, allowing for later volatile release times and less volatile breakthrough.

While CFD models are extremely useful and take into consideration much of the complex mechanisms of solid particle combustion they are also very computationally intensive and costly. Simpler models can be useful for predicting trends and understanding fundamental principles involved in flame length. The purpose of these types of models is not necessarily to accurately predict the length but to gain insight into how various parameters impact flame length. Kim et al. [24] created a model that could theoretically predict flame length of single coal particles in a laminar flow reactor (LFR). Their model is based on balancing mass using a char oxidation rate equation and numerically solving for a burn-off temperature of a particle. Once the particle reaches this burn-off temperature it is said to be the tip of the flame for this study. Using a spatial variation curve for particle temperature fitted to measured data, flame length could be predicted for a given burn-off temperature. While the model is fairly simple and promising for theoretical

prediction of flame length, it requires experimental data of the particle temperature across the flame and is only applicable to laboratory-scale entrained laminar flow reactor systems. Because of this and the complexity of the problem analytical models that predict solid fuel flame length for a wide range of burner sizes and fuels do not currently exist.

3 BACKGROUND

A flame length model for particle laden flows was initially developed by Owen et. al. [3]. This chapter will review the theory and development of his model as a foundation for improvements and additional validation to be presented in this work. The chapter begins by defining a flame and what is typically meant by a flame length. Following this description the model is then derived. The meaning of each variable and its contribution to the model is discussed. The processes of NO_x formation, carbon burnout will be discussed along with the impact of swirl on flame shape and length.

3.1 Flame Length Description

A flame is defined as a region over which fuel and oxidizer are converted to products. Flame thickness, or the physical distance over which a flame reaction occurs is typically on the order of millimeters. These thin reaction zones form flame sheets, clusters, or wrinkled layers which surround regions of unburned fuel which are much larger in scale. Thus, a Bunsen burner flame is a thin annular sheet about 1-2 mm in thickness surrounding a fuel jet several cm in length. The flame length, unlike the flame thickness is the distance from the burner or fuel exit to the farthest axial distance where the flame sheet is located. In practice this location is always somewhat transient, moving closer or further from the burner tip due to perturbations in the flow and reaction rates.

Flame lengths are important for both practical and analytical reasons. In some applications, a flame is used to transfer heat to a surrounding surface such as the glass making process. The flame length is therefore an important design parameter and should be made to match the length of the desired heated surfaces. In other applications the flame may be used to produce a hot gas such as in a gas turbine engine. Here the flame should be as short as possible in order to reduce the size and weight of the engine. When a flame impinges on a wall, reactions can be quenched resulting in undesirable pollutants and perhaps melting or corrosion of the impacted surface. A knowledge of and the ability to predict flame length can therefore be very important.

Flame length has been measured by various methods including visual observation, imaging of visible radiation, temperature measurement, and species measurement. Solid particle flames provide an additional complication for determining flame length because both the gaseous volatiles and the solid particles can produce radiation which results in visible emission. In this work, the flame length was measured by visual observation of the luminous sooting region of solid particle flames. Soot is produced by the volatile fraction of the fuel and therefore a visible indication of soot measures only the volatile portion of the flame. Many of the fuel / burner operating conditions produced particles emission well beyond the volatiles flame length. This length was not recorded or included in the flame length.

Flame lengths are typically modeled by determining the location where a fuel/oxidizer mixture is stoichiometric or the mixture fraction of the gases is stoichiometric. The flame length model developed is therefore an estimate of the length required to mix the volatile fuel with enough oxidizer to be stoichiometric as has been done for other flames as explained by Turns

[25] for laminar and turbulent jet flames and for swirled gaseous flames by Chen and Driscoll [17].

3.2 Model Derivation

The model as presented here was initially derived by Owen [3] but is repeated here for clarity and as a starting point for modifications to be added in this work. The model begins with the stoichiometric ratio of fuel to oxidizer being set equal to a constant c_s and shown in Equation 3.1 where $\dot{m}_{ox}$ is the total mass flow rate of oxygen in the oxidizer and $\dot{m}_{fuel}$ is the total mass flow rate of fuel.

$$c_s = \left(\frac{\dot{m}_{fuel}}{\dot{m}_{ox}}\right)_s \tag{3.1}$$

The numerator and denominator can be expanded as shown in Equation 3.2. The numerator represents the fuel flow entering through the primary annulus which for the burner being used is between the primary tube diameter d_p and the center tube diameter d_c, where ρ_{mix}, is the primary fuel-air mixture density, V_P is the primary mixture velocity, and $Y_{fuel,p}$ is the fuel mixture fraction of the primary flow. Section 4.1 includes a diagram of the burner being used and an explanation of where each stream is located.

The denominator consists of four terms each representing a flow of oxygen into the fuel rich region. The first term follows the nomenclature of Chen and Driscoll [17] and expresses the radial velocity (U_{RZ}) along the axial circumference ($\pi b L_f$) of the flame. L_f is the flame length, b is the theoretical diameter of the recirculation zone core estimated to be approximately 80% of the secondary tube diameter, ρ_{sec} is the density of the secondary air stream and $Y_{O_2,sec}$ is the mass fraction of O_2 in the secondary stream. The magnitude of U_{RZ} was determined as a function

of swirl, S, and secondary axial velocity, V_{sec}, based on a correlation of the data from Chen and Driscoll as shown in Equation 3.3. This correlation was not provided by Chen and Driscoll but was developed by fitting data from their work relating U_{RZ} to swirl. The constant c_2 will be evaluated by experimental results to be shown later.

$$c_s = \frac{\rho_{mix} V_p \frac{\pi}{4}\left(d_p^2 - d_c^2\right) * Y_{fuel,p}}{Y_{O_2,sec}\left[\rho_{sec}\pi b L_f U_{RZ} c_2 + \rho_{sec}\left|V_p - V_{sec}\right| d_p L_f \pi c_1\right] + \dot{m}_{O_2,c} + \dot{m}_{O_2,p}} \tag{3.2}$$

$$U_{RZ} = \frac{0.23 * S^4 * V_{sec}}{0.004 + S^4} \tag{3.3}$$

The second term in the denominator represents oxygen mixing into the fuel jet due to shearing created by the axial velocity difference between the fuel jet and the secondary flow. The rate of mixing is assumed to be proportional to the absolute value of the velocity difference of V_p and V_{sec}, which has been experimentally observed for turbulent flames. The constant c_1 must also be determined by experimental data.

The third term in the denominator $\dot{m}_{O_2,c}$ is the flow rate of oxygen in the center tube. The model assumes that all of the oxygen delivered from this tube is mixed into the fuel stream. In the experiments used to develop this correlation, the flow exiting this center tube contained pure oxygen.

The final term in the denominator $\dot{m}_{O_2,p}$ is the oxygen contained in the primary stream. For safety reasons, the oxygen concentration in the primary flow must be maintained near that of air but in some of the data used to develop the correlation, pure oxygen was premixed into the primary air-fuel stream within the last 10 cm prior to the burner exit.

Rearranging the terms of Equation 3.2 to solve for the flame length produces Equation 3.4. The constants c_1 and c_2 were initially found by minimizing a least squares

difference between the measured and predicted flame lengths for each fuel. This provided fuel specific correlations for flame length.

$$L_f = \frac{\frac{\dot{m}_{fuel}}{c_s} - \dot{m}_{O_2,p} - \dot{m}_{O_2,c}}{\left[\rho_{sec}\pi b U_{RZ} c_2 + \rho_{sec}\left|V_p - V_{sec}\right| d_p \pi c_1\right] Y_{O_2,sec}} \tag{3.4}$$

3.3 Formation of Nitric Oxides (NO_x)

NO_x is mainly composed of NO which is formed by three chemical mechanisms namely thermal, prompt, and fuel NO_x. Thermal NO_x occurs as N_2 and O_2 dissociate at very high temperatures (above 1800 K). Atomic N and O then react in what is commonly known as the extended Zeldovich mechanism [25] shown in Equations 3.5 through 3.7. Previous work at BYU found that this combustor never exceeds 1800 K outside the flame [26],where the residence time is long enough to produce the reaction; therefore, this pathway for NO formation is thought to be negligible.

$$O + N_2 \rightarrow NO + N \tag{3.5}$$

$$N + O_2 \rightarrow NO + O \tag{3.6}$$

$$N + OH \rightarrow NO + H \tag{3.7}$$

Prompt NO_x occurs very quickly within a flame, and thus its name. CH radicals form very rapidly during combustion and proceed to react with N_2 in the Fenimore mechanism [25] shown in Equations 3.8 and 3.9. The cyanide compounds formed will proceed to form intermediate compounds which eventually result in NO. At richer equivalence ratios (> 1.2) HCN will follow the chain sequence shown in Equations 3.10 through 3.13 to form NO. This mechanism is thought to contribute to only a small fraction of the NO formed in particle laden flames because the concentrations of HCN produced are lower than that produced by fuel NOx.

$$CH + N_2 \rightarrow HCN + N \quad (3.8)$$

$$C + N_2 \rightarrow CN + N \quad (3.9)$$

$$HCN + O \rightarrow NCO + H \quad (3.10)$$

$$NCO + H \rightarrow NH + CO \quad (3.11)$$

$$NH + H \rightarrow N + H_2 \quad (3.12)$$

$$N + OH \rightarrow NO + H \quad (3.13)$$

Fuel NO_x is the dominating mechanism in biomass and coal combustion. Nitrogen is contained in the fuel's molecular structure which will quickly convert to HCN or ammonia (NH_3). These products will then follow a path similar to the prompt mechanism outlined above. It is assumed that this is where the majority of NO_x comes from in this work.

3.4 Loss on Ignition (LOI)

Beyond the volatile combustion region, solid fuel particles continue to react in a process known as char oxidation. To measure the degree of burnout of solid particles after char oxidation ASTM procedure D3748 was used to determine loss on ignition (LOI), which is an approximate measure of the amount of carbon left in the ash. The procedure involves heating solids in air at high temperature. For a detailed step-by-step outline of the ASTM procedure, refer to APPENDIX A. The majority of the mass released is carbon which oxidizes to produce CO and CO_2. There may however be some mass loss for other elements such as sulfur. LOI is reported as a fraction of the remaining ash or as a percentage of the mass of the remaining ash. When the ash fraction of a fuel is very low as is the case for wood, the amount of carbon remaining in the ash may be a very small fraction of the initial fuel carbon (high burnout) but may still be a large

fraction of the remaining ash (high LOI). The smaller the ash fraction, the more difficult it is to obtain low LOI.

During char oxidation carbon on the surface of the particle reacts with oxygen to form CO and CO_2 via global reactions [25] as shown in Equations 3.14 through 3.17. After immediate oxidation CO concentration is generally high on the surface of the particles. CO will diffuse away from the surface and further react with oxygen to form to CO_2 as shown in Equation 3.18, which becomes the final product of carbon in the char.

$$C + O_2 \rightarrow CO_2 \tag{3.14}$$

$$2C + O_2 \rightarrow 2CO \tag{3.15}$$

$$C + CO_2 \rightarrow 2CO \tag{3.16}$$

$$C + H_2O \rightarrow CO + H_2 \tag{3.17}$$

$$CO + \frac{1}{2}O_2 \rightarrow CO_2 \tag{3.18}$$

The char oxidation rate is controlled by either temperature (kinetic control) or the diffusion of oxygen to the surface (diffusion controlled). While both modes can occur in a particle laden flame, diffusion controlled oxidation tends to dominate until particles become isolated and cool rapidly in the post flame region. In experiments for this work, once particles leave the reactor, gas and particle temperature drop rapidly quenching reactions. In fuel rich regions, char oxidation is reduced as oxygen is consumed by the volatiles more rapidly than by the char. Thus char oxidation occurs predominantly after the volatile flame and before exiting the reactor or in the post flame region of the reactor. The final degree to which char oxidation has progressed by the end of the reactor depends on residence time in this post flame region. Owen [3] showed that LOI is correlated with flame length. In a fixed volume reactor increasing volatile

flame length decreases the length of the burnout zone which reduces the residence time for char oxidation.

4 EXPERIMENTAL SETUP

This chapter describes the experimental facilities and equipment used to obtain data for this work, including NO_x, LOI, and flame length measurements. ASTM fuel analyses are also listed for each solid fuel here.

4.1 Combustion Facility

All experiments were performed in a 150 kW_{th}, cylindrical, down-fired Burner Flow Reactor (BFR). The full schematic is shown in Figure 4.1. The BFR has an inside diameter of 0.75 m and a height of 2.4 m which consists of six burner sections with heights of 0.4 m. Each section has four 90 mm x 290 mm access ports 90 degrees apart from one another. Flame length was observed visually through quartz windows mounted in the access ports on the south side of the reactor. The windows allowed observation of a large portion of the axial distance of the flame but the flame was not visible in some locations between windows.

Measurements for this work include exhaust gas concentrations, ash burnout (LOI), and volatile flame length and are summarized in Table 4.1. Exhaust gas concentrations were measured using a PG-250 Horiba gas analyzer. This analyzer was capable of measuring NO_x, CO, CO_2, and O_2. The analyzer was calibrated at the beginning of each day of testing to ensure accuracy. The exhaust gas line went through an ice bath to condense water before entering the analyzer. Ash samples were collected on a metal plate at the bottom of a barrel below the

cyclone from which LOI measurements were obtained. Volatile flame length was measured by visual observation via glass windows mounted onto the access ports of the BFR. The windows were regularly blown off with pressurized air from the inside to improve visibility.

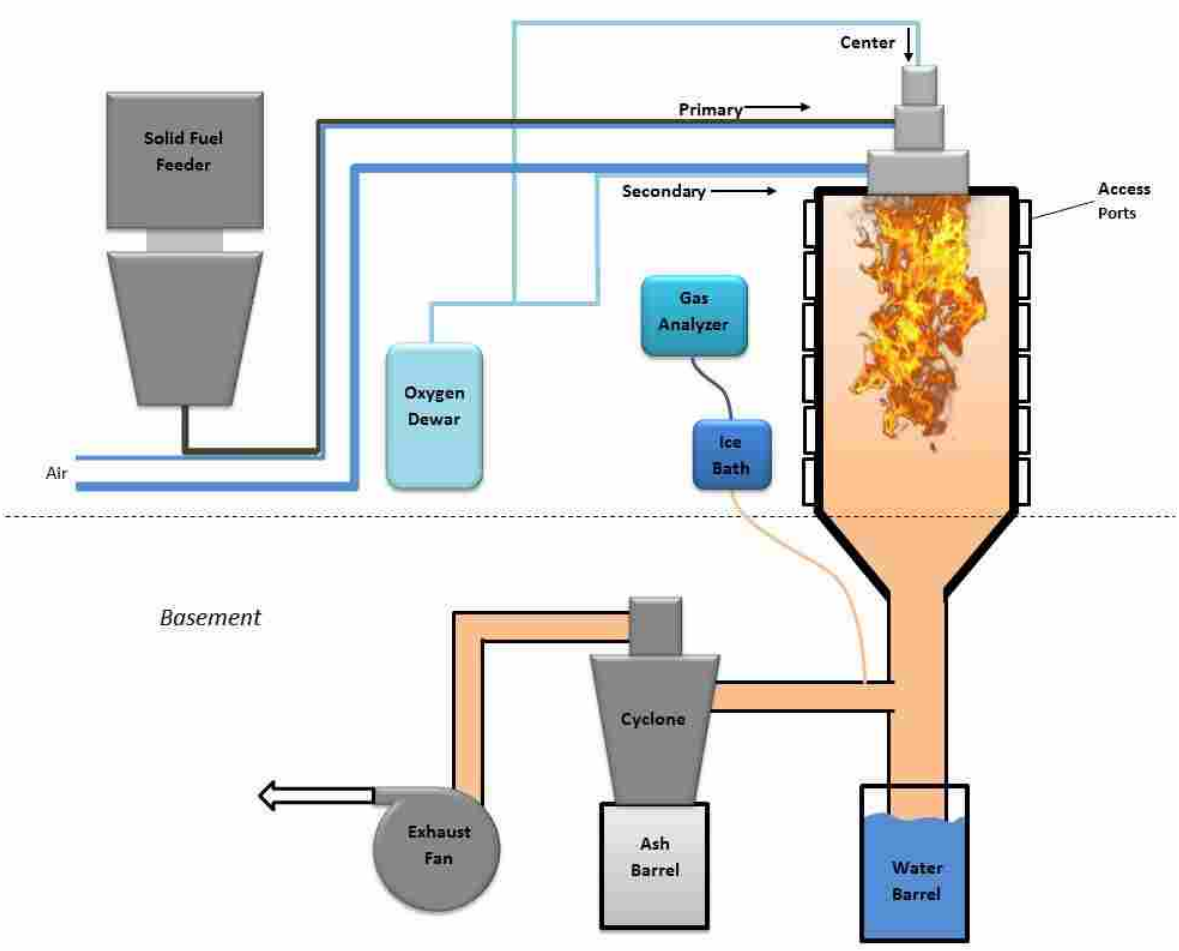

Figure 4.1: Schematic of BYU combustion facility and equipment (not to scale)

Table 4.1: Measurements taken at each operating condition and associated methods

Measurement	Units	Method
NO	ppm	PG-250 Horiba gas analyzer
CO	ppm	
CO_2	% vol	
O_2	% vol	
LOI (Loss on Ignition)	% mass	ASTM Procedure D3748 (See Appendix A)
Flame Length	meters	Visual Confirmation

For this work a variable-swirl burner designed by Air Liquide was employed. The burner consisted of three coaxial tubes allowing for three separate inlet flows, as shown in Figure 4.2. The diameter of each of the three tubes may be varied by exchanging tubes. Diameters are shown in Table 4.2 where S, M, and L stand for small, medium, and large respectively. Channel 1 (center) is typically used for the natural gas during preheating. Channel 2 (primary) is typically used for solid fuel addition conveyed with air from a bulk bag feeder. Channel 3 (secondary) is used for the secondary air flow that is swirled prior to entering the annulus in a variable swirl block above the outlet.

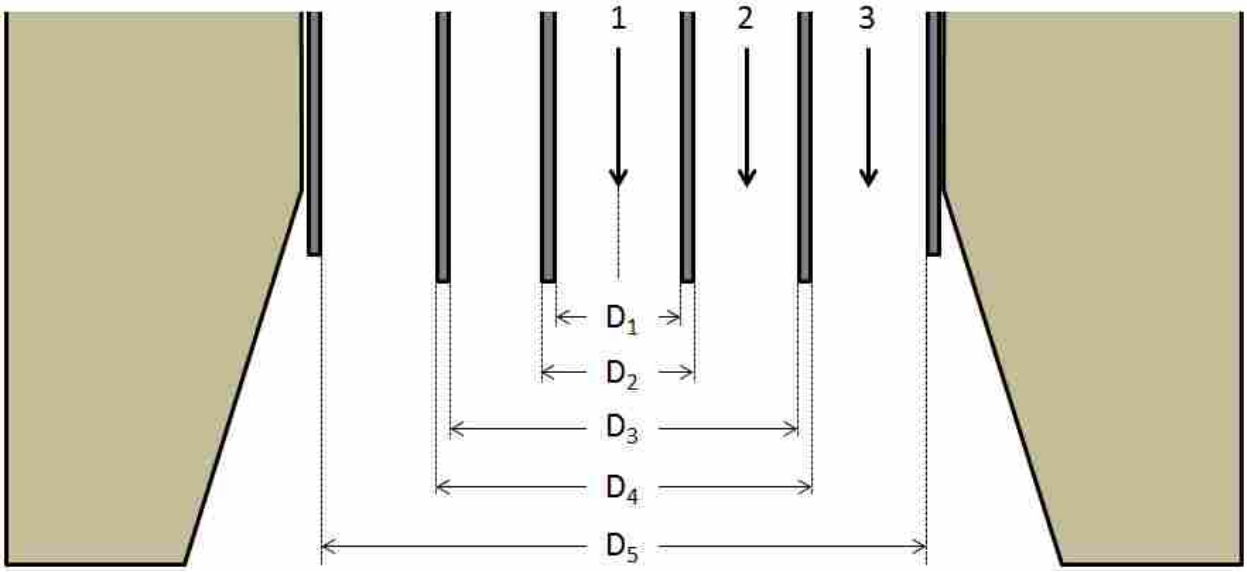

Figure 4.2: Cross section of Air Liquide burner (not to scale)

Table 4.2: Diameters (cm) of each of the tubes in the Air Liquide burner

	S	M	L
D_1	1.905	2.858	3.505
D_2	2.667	3.340	4.216
D_3	4.272	N/A	5.479
D_4	4.826	N/A	6.033
D_5	10.795	N/A	13.335

4.2 Fuel Analyses

Data for five solid fuels: medium particle size hardwood, fine particle size hardwood, straw, switchgrass, and sub-bituminous coal, were used in this work. The data for hardwoods and straw were previously taken by Owen [3]. The ASTM proximate and ultimate analyses of the five fuels are displayed in Table 4.3.

Table 4.3: Proximate and ultimate analysis (as received), heating value, and mean particle size of five solid fuels

Proximate (as received, wt %)	Medium Wood	Fine Wood	Straw	Switchgrass	PRB Coal
Moisture	5.28	5.83	7.15	8.26	21.23
Ash	0.3	0.54	4.56	11.6	5.53
Volatiles	79.06	76.42	73.81	67.78	33.76
Fixed Carbon	15.36	17.21	14.48	12.36	39.48
Ultimate (as received, wt %)					
H	5.40	5.36	5.68	4.14	2.06
C	49.85	49.87	47.30	39.10	54.39
N	0.26	0.32	0.54	0.16	0.86
S	0.09	0.10	<0.01	0.13	0.26
O	38.82	38.82	41.60	36.61	15.67
HHV (kJ/kg)	17,638	17,638	17,069	15,166	22,048
Mean Size (μm)	421	138	347	432	50

The four biomass fuels have similar proximate and ultimate analyses while the coal analyses are significantly different. The nitrogen content of the coal is the largest of all fuels being approximately three times the value for wood. The volatiles fraction for coal is about half that of the biomass fuels. It should also be noted that three of the fuels have similar particle size (medium wood, straw and switchgrass) while the fine wood is about half the mean diameter of these three and the coal is significantly smaller than all biomass fuels.

4.3 Operating Conditions

Various operating conditions were used for experiments in this work and are summarized in Table 4.4. The burner configuration 1S2L3L was chosen for these tests because it was the most frequently used configuration in Owen's data allowing for a more suitable comparison between fuels. Oxygen varied from 0 – 16 kg/hr for switchgrass, but only 0 – 8 kg/hr for coal. This is because at oxygen flow rates above 8 kg/hr in the center tube the high velocity of oxygen would overtake the coal flame, which is already shorter than any biomass flame, in which the oxygen flow appeared to destroy the recirculation zone and lead to poor results. Swirl was held at three different values depending on the number of 360 degree turns of the adjusting screw in the swirl block. Oxygen addition occurred in both the center tube and secondary flow. In the secondary flow two cases existed. For the "Constant Air" case oxygen was simply added to the secondary air flow. For the "Constant O_2" case the secondary air was reduced in order to keep the total mass flow of oxygen into the reactor constant. In other words, since air is made up of almost 25% oxygen by mass, the secondary air flow would be reduced by about 4 kg/hr for each kg/hr of additional oxygen flow.

Table 4.4: Test matrix of operating conditions

Fuel	Burner Configuration	O_2 Flow Rates (kg/hr)	Swirl (0, 6, 9 Turns)	Oxygen Location
Switchgrass	1S2L3L	0, 2, 4, 6, 8, 12, 16	1.44, 1.11, 0.84	Center, Secondary (Constant Air, Constant O_2)
Coal	1S2L3L	0, 4, 8	1.44, 1.11, 0.84	Center, Secondary (Constant Air)

In addition to the data taken at BYU, two data points from the University of Utah were included for comparison. The first data point was taken in their L-1500 furnace. This is a 1.5 MW combustor similar to the BFR which employs a burner with coaxial tubes for firing

pulverized coal and/or natural gas. This particular data point was taken with pulverized coal, similar to that used in BYU tests, fired in air with a swirl number of approximately 1.2. The second data point was taken in their Oxy-Fuel Combustor (OFC). This is a 100 kW combustor with no swirl capabilities. This data point was also taken with pulverized coal, but fired with an O_2/CO_2 mixture instead of air. Thorough descriptions and images of these combustors are available on the University of Utah's Institute for Clean and Secure Energy website [27].

5 RESULTS AND DISCUSSION

Experimental results for nitric oxide (NO) concentration and loss on ignition (LOI) tests are presented in this chapter. Similar results and trends were previously presented by Owen et al. [3] for wood and straw. Results for two additional fuels (switchgrass and coal) are added to his data and discussed. The flame length model presented by Owen is compared to all of the data and refinements to the model are then presented. The influence of various burner design parameters are then investigated using the model and the data.

5.1 NO vs. LOI

NO and LOI measurements were taken while burning switchgrass and coal, the results of which are shown in Figure 5.1. A trade-off curve, similar to the results obtained by Owen [3] was observed between NO and LOI where NO was reduced as LOI increased. The total burn time for a particle in the reactor can be divided into two components, the flame or reducing zone and the burnout or oxidizing zone. Generally, as oxygen flow increases flame length or reducing zone decreases and the burnout zone or oxidizing zone increases. As the reducing zone decreases, the opportunity to reduce fuel nitrogen to N_2 is reduced and the amount of oxidized nitrogen or NO increases. Similarly, as oxygen is added and the burnout zone increases, LOI decreases.

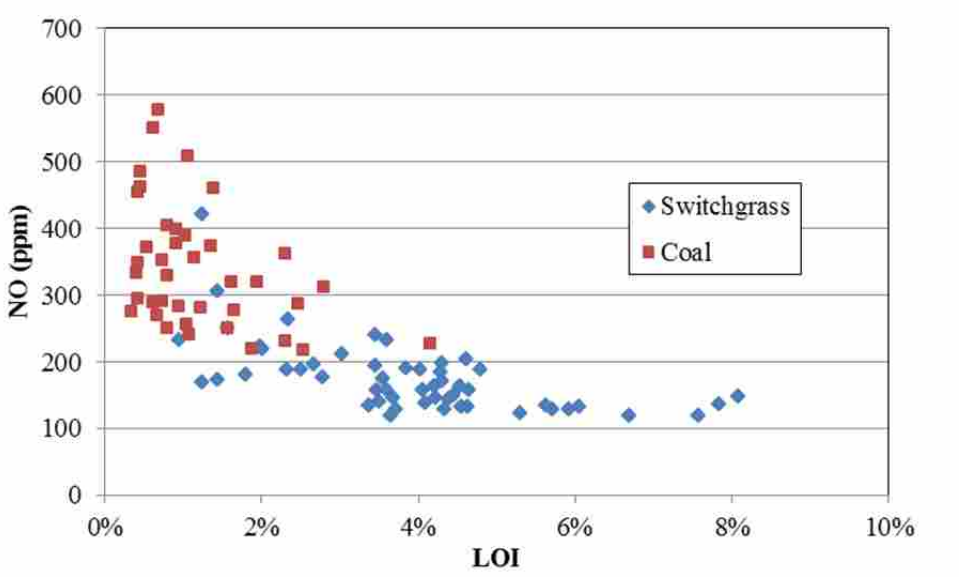

Figure 5.1: NO vs LOI for two fuels (switchgrass and coal) at various swirl values and oxygen addition levels with burner configuration 1S2L3L

Data for all five fuels are shown in Figure 5.2. The wood fuels have very low ash fractions which tend to produce higher LOI. They also have large particles and high volatile fractions which should produce longer fuel rich zones and more NO reduction. Thus wood is located on the high LOI, low NO end of the trade-off curve. The coal has a larger ash fraction and a smaller particle size which tends to produce low LOI. The lower volatile content and smaller size should also produce a smaller fuel rich reducing zone which results in higher NO. This causes coal to be on the high NO, low LOI end of the trade-off curve. It is surprising that although coal and wood contain very different amounts of nitrogen and ash, both fuels fall on a similar NO-LOI trade-off curve.

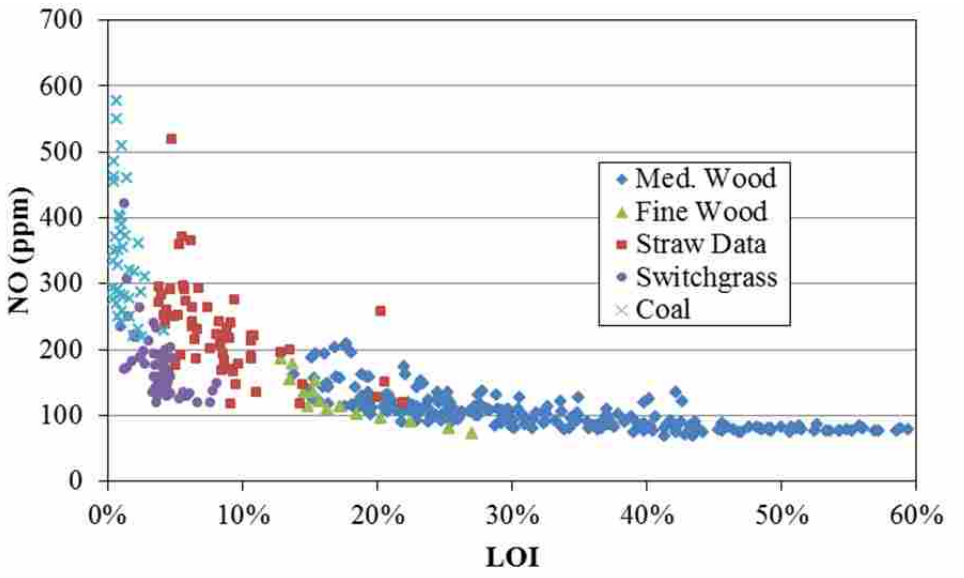

Figure 5.2: NO vs LOI for all fuels at various operating conditions

The straw and switchgrass NO-LOI trade-off curves are between the coal and wood fuels with the straw tending to produce an overall worse trade-off or a curve further from the origin while the switchgrass has a better trade-off or closer to the origin. Based on this particular measure, the switchgrass is the best fuel measured. This may be because the switchgrass has a high ash fraction which produces low LOI and a low nitrogen content which enables lower NO. Biomass fuels have a challenge to produce low LOI because of the large volatile fraction and larger particle size producing a longer fuel rich region and smaller burnout zone, while requiring more time to burn out large particles.

5.2 NO vs CO

A comparison of exhaust CO and NO concentration for all fuels is shown in Figure 5.3. These data indicate that for a given fuel, NO decreases approximately linearly with the increasing log of CO concentration. Increasing CO is another indication of a large reducing zone and short burnout zone for char particles. Thus CO and LOI are similar indicators of long flames,

or short oxidizing zones. At a fixed exhaust CO the wood produced the lowest NO and the coal and straw the highest NO. This appears to be somewhat correlated with nitrogen content in the fuel. Straw produced the highest CO in comparison to the other fuels with none of the operating conditions being able to produce less than 100 ppm.

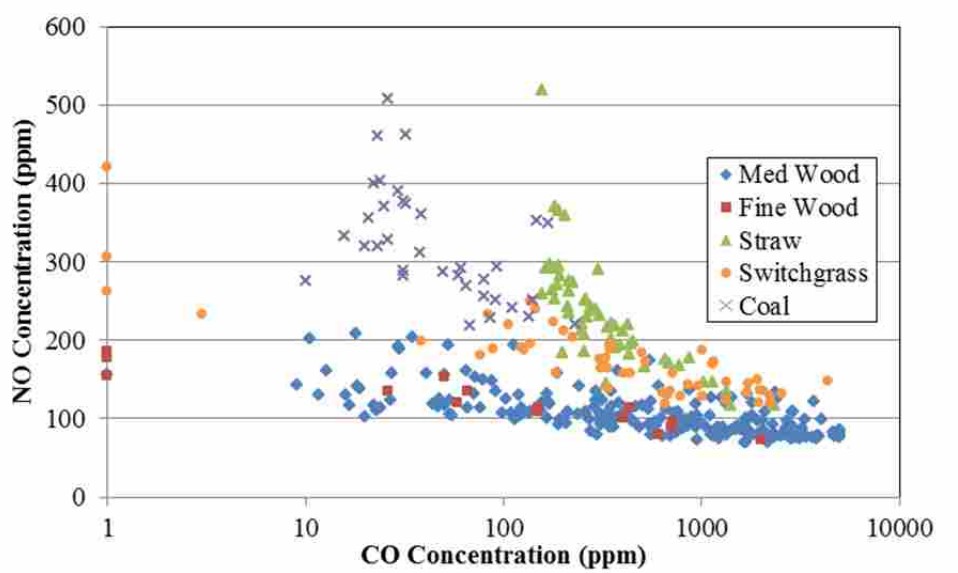

Figure 5.3: NO vs CO for all fuels at various operating conditions

5.3 LOI vs Flame Length

Figure 5.4 shows how LOI varies compared to flame length for all fuels. Although there is a high amount of scatter, within a given fuel, there is a trend of increasing LOI with increasing flame length. As discussed earlier, this is attributed to a shorter oxidation zone for longer flames. These data show more clearly that the high LOI is correlated with the wood fuels which are very low ash fuels. The carbon in the fuel can be almost completely burned out but because there is only a small amount of ash, the carbon remaining is a significant fraction of the total mass remaining. It is more difficult to produce low LOI with a low ash fuel. Straw and switchgrass

have higher ash content and therefore lower LOI than wood but the larger particle size contributes to higher LOI than coal which has both high ash content and small particle size.

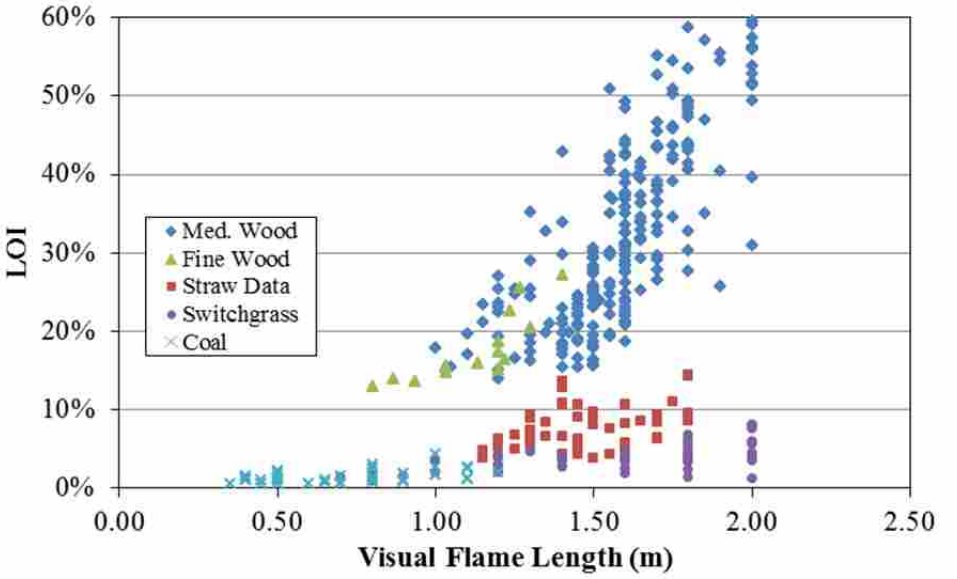

Figure 5.4: LOI vs visual flame length for all fuels at various operating conditions

Lower LOI usually indicates higher burnout percentages. However Figure 5.5 demonstrates that straw and switchgrass have lower burnout in spite of their low LOI. This is first due to the large ash content of these two fuels as discussed previously, as well as large particles which take longer to burnout.

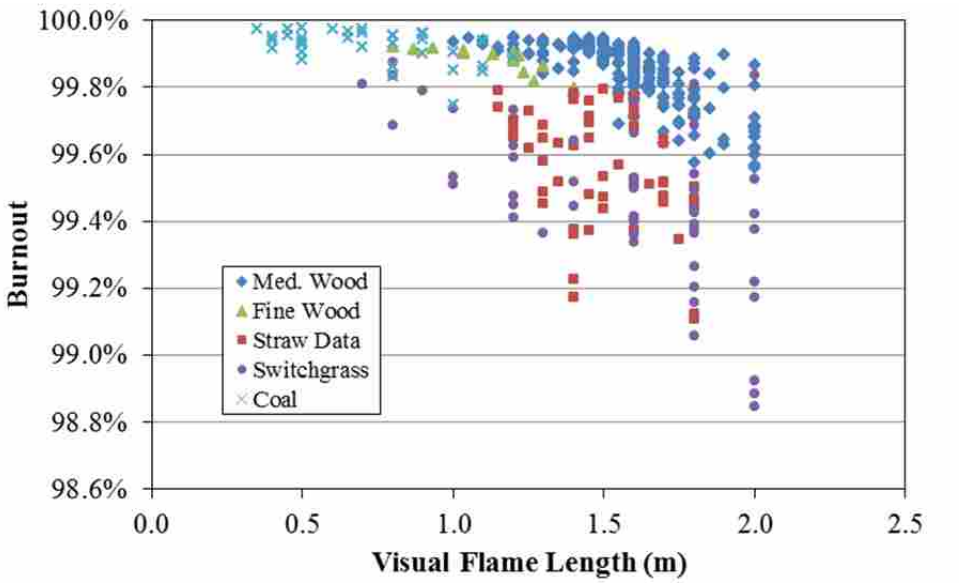

Figure 5.5: Burnout vs visual flame length for all fuels at various operating conditions

The coal and switchgrass data are shown on a finer scale for LOI in Figure 5.6. At this scale, the switchgrass data do not appear to correlate well with flame length. In order to investigate the lack of correlation with this fuel, Figure 5.7 identifies various operating conditions used with switchgrass These include high and low swirl and holding secondary air flow constant, "constant air," versus holding the total oxygen flow constant, "constant O_2". The figure shows that it is primarily the data for constant O_2 flow rate that do not correlate with flame length. For these data, the flow of secondary air is significantly reduced creating a poor mixing between fuel and oxidizer which lengthens the flame but the oxygen concentration in the burnout zone is significantly increased because nitrogen as a diluent has been reduced and the residence time has increased because of a lower total volume flow rate. This higher O_2 concentration and longer residence time help reduce LOI.

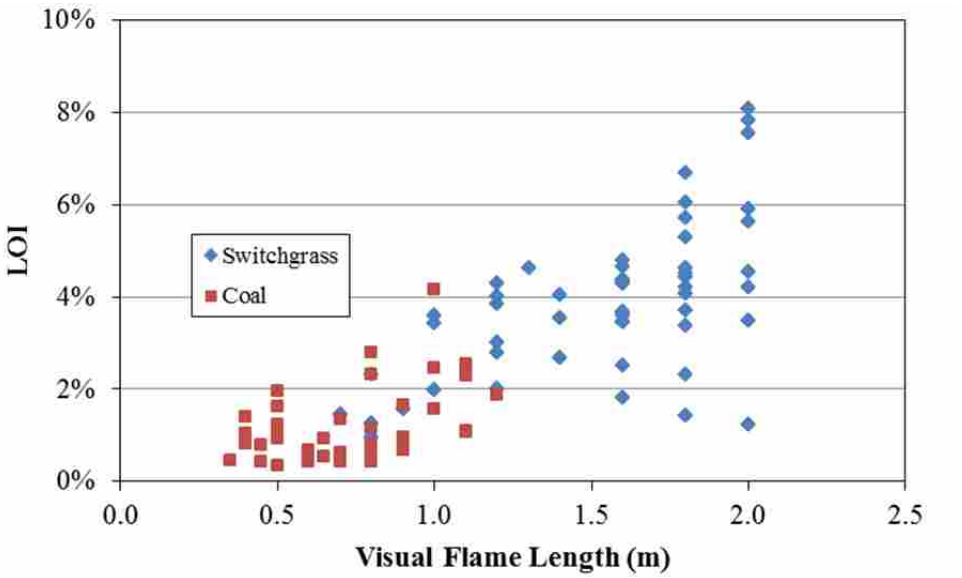

Figure 5.6: LOI vs visual flame length for switchgrass and coal at various swirl values and oxygen addition levels with burner configuration 1S2L3L

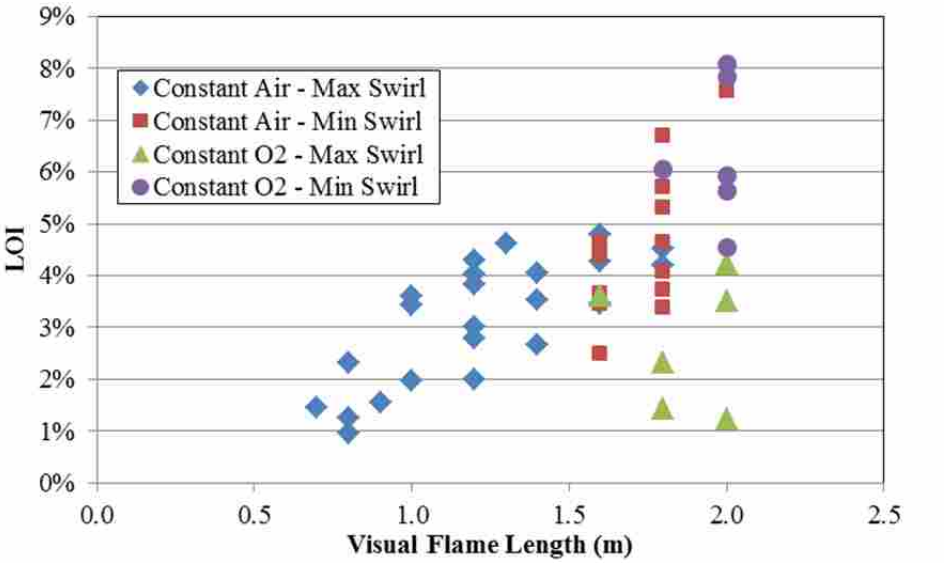

Figure 5.7: LOI vs visual flame length for switchgrass data

In "Constant Air" experiments the secondary air flow was held constant while oxygen enrichment levels varied. In this case the total flow rate is not changing dramatically and the recirculation zone remains at approximately the same strength for each data point while oxygen

concentration of the secondary is increased. This method of changing flame length produced the trade-off consistent with all of the other data. The trend is most clear for the Maximum Swirl case while the Minimum Swirl data are more scattered. In the Minimum Swirl case the lowered swirl causes the flame to extend almost the entire length of the reactor. Swirl has a stronger influence on flame length than oxygen addition to the secondary air.

In "Constant O_2" experiments total oxygen mass flow into the BFR was held constant. Thus the secondary air flow decreased dramatically when pure oxygen was added to the secondary. This decreases flow velocity and recirculation zone strength which reduced mixing and created longer flames. It is these data for which LOI does not correlate with flame length. Because the sum of oxygen in the air and pure oxygen is constant, the post flame O_2 concentration is not changed significantly. One possible explanation for why LOI did not increase with increased flame length is a longer residence time produced by lowered secondary air flow.

5.4 NO vs Flame Length

Figure 5.8 shows how NO concentration varies with flame length for all fuels. The two new fuels (switchgrass and coal) lie along a similar trend line to medium wood while straw produces more NO for a given flame length than the other fuels. It is not clear why the straw has higher NO for the same flame length but may be caused by higher fuel nitrogen.

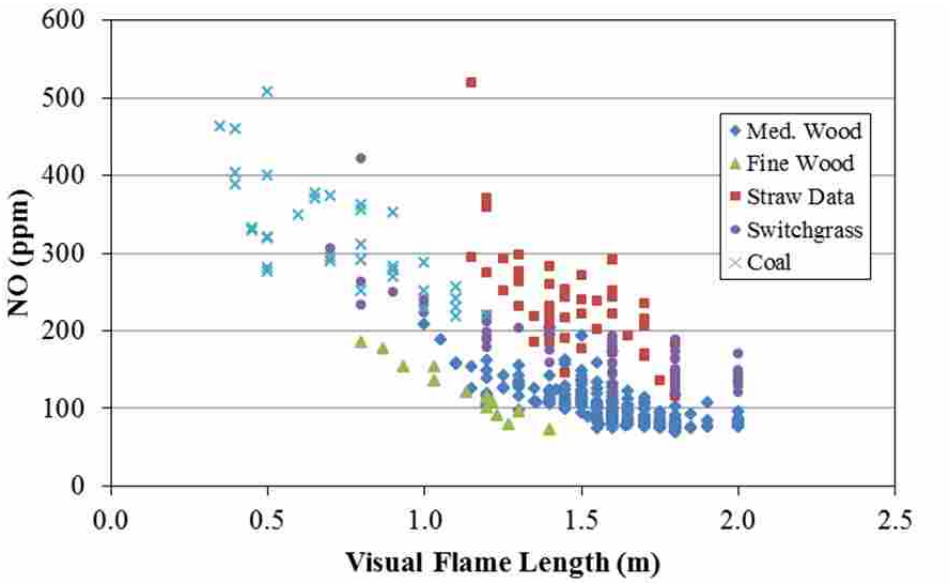

Figure 5.8: NO vs visual flame length for all data at various operating conditions

5.5 Measurement Comparison

The accuracy of the model developed previously was evaluated for all of the data including the two new fuels investigated in this work by comparing calculated flame length with the visually measured flame lengths as shown in Figure 5.9. Proportionality constants, c_1 and c_2, were found by a best fit to the data and are unique values for each fuel.

Two data points have been added from data collected by the University of Utah. "Utah OFC" refers to a 50 kW, oxy-combustion case with no swirl [28]. "Utah L1500" refers to a 1.5 MW, air-fired cased with an estimated swirl of 1.2 [29]. Both cases used bituminous coal similar to that used in the BYU experiments but coal property data were not available. c_1 and c_2 were fit to the data for the L1500 case and then used for both the L1500 and OFC cases. The L-1500 is an exact match because the constants were selected to make it fit but the OFC flame length is surprisingly well predicted with these constants given that the two cases are so different in burner size, swirl amount, and oxidizer setup.

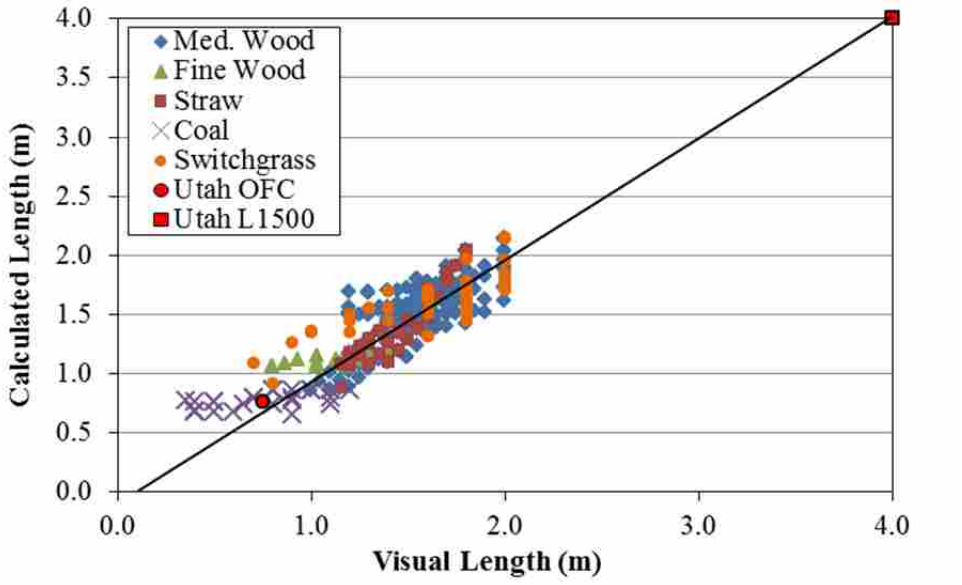

Figure 5.9: Calculated flame length vs. visual flame length for all data by fuel

Most of the fuels follow a slope reasonably well predicted by Owen's model but the slope of the coal data are noticeably flatter than the other fuels. There are no combinations of c_1 and c_2 that produce a steeper slope. All of the fuels tested by Owen are biomass fuels with high ASTM volatile fractions while the coal volatile fraction is significantly lower. Because the measured flame length is related to the volatile fuel flame and not the total fuel it was thought that the model might be more accurate if the volatile flow rate, not the total fuel flow rate, was used.

5.6 Volatiles Flame Length

The flame length model is based on calculating the distance from the burner where the fuel oxidizer ratio is stoichiometric. The amount of fuel is therefore critical to determining the flame location. For the original model produced by Owen [3]the total mass of the fuel including volatiles and solid fractions was used. The flame however is actually located at the boundary where the volatile fuel to oxidizer mixture is stoichiometric. A visible flame is produced by

radiating soot particles indicating the oxidation of gaseous fuel rich pyrolysis products. The flame is expected to be located where the volatile fuel reacts, not the solid fuel. Using the volatile fuel fraction is therefore more consistent with the visual measured flame value than inclusion of the total fuel mass.

In order to correct for this shortcoming in the previous model, the mass flow term was multiplied by the volatiles fraction (f_v) obtained from the ASTM Proximate Analysis resulting in Equation 5.1. While more complex models could be used to obtain the volatile fraction such as the Coal Percolation and Devolatilization (CPD) Model [30] or FLASHCHAIN [31] the ASTM results are readily available for most fuels and the fidelity is consistent with the rest of the model.

$$L_f = \frac{\frac{\dot{m}_{fuel} f_v}{c_s} - \dot{m}_{O_2,p} - \dot{m}_{O_2,c}}{\left[\rho_{sec}\pi b U_{RZ} c_2 + \rho_{sec}\left|V_p - V_{sec}\right| d_p \pi c_1\right] Y_{O_2,sec}} \tag{5.1}$$

This model was again fit to experimental data to determine new values of c_1 and c_2 for each fuel. Figure 5.10 shows the comparison of calculated and visual flame lengths with the inclusion of the volatiles fraction in the model. Using the volatiles fuel flow clearly improves the correlation of the coal but slightly increases the scatter in the biomass and Utah data. The values of R^2 were calculated for both the original ($R^2 = 0.7707$) and this modified model ($R^2 = 0.7591$) and it was found that R^2 decreased by 0.0116.

The model assumes that oxygen in the fuel carrier gas and the center tube are perfectly mixed at the burner exit. Clearly this is not the case as it takes some distance for the two streams to mix. For coal the volatile fraction is small and the amount of oxygen required to reach stoichiometric is the lowest of all the fuels. This makes the perfectly mixed assumption less valid and the model is less predictive. When the flow of pure oxygen in the center tube approaches stoichiometric the model cannot be valid. For example, at 8 kg/hr the model predicts a very short

flame length of 0.2 m. This is approximately the length of 4 primary burner diameters which is too short for the oxygen to mix with the fuel. Predicted values of 4 burner diameters or less should not be considered valid and are not shown in Figure 5.10.

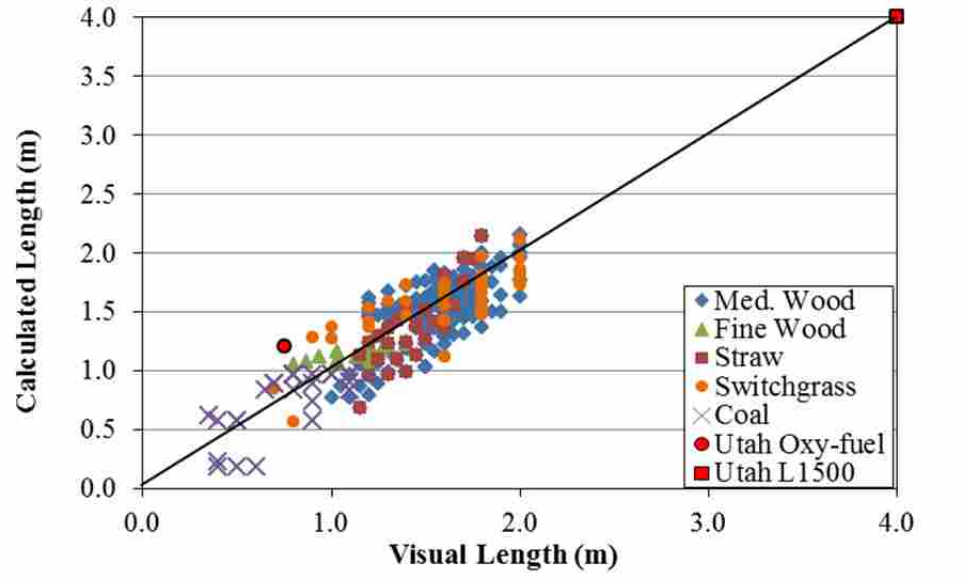

Figure 5.10: Calculated volatiles flame length vs. visual volatiles flame length for all data by fuel

5.7 Trends in Flame Length Suggested By Model Results

The model was used to understand trends in burner design variables by changing one variable while holding all other variables constant. Some variables had little effect while others were much more significant. Results were obtained for each fuel but only those for medium wood are shown because of the larger number of experimental results available to compare with the model.

5.7.1 Primary Fuel Tube Diameter

Figure 5.11 shows the trend in flame length produced by the model as the primary diameter was changed. The legend shows the size of the three burner tubes as described in Figure 4.2 and Table 4.2. For example, 1S2X3L indicates the first tube or center tube was set to the dimensions of the smaller of the three center tubes in the model, the second tube or primary tube is variable in the model (X) and the third tube or outer secondary tube was set in the model to the dimensions of the larger of the two secondary tubes. Two burners or two sets of center and secondary tubes were modeled, each with a variable primary tube diameter. Results of the measured flame length for the given configurations are also shown for comparison.

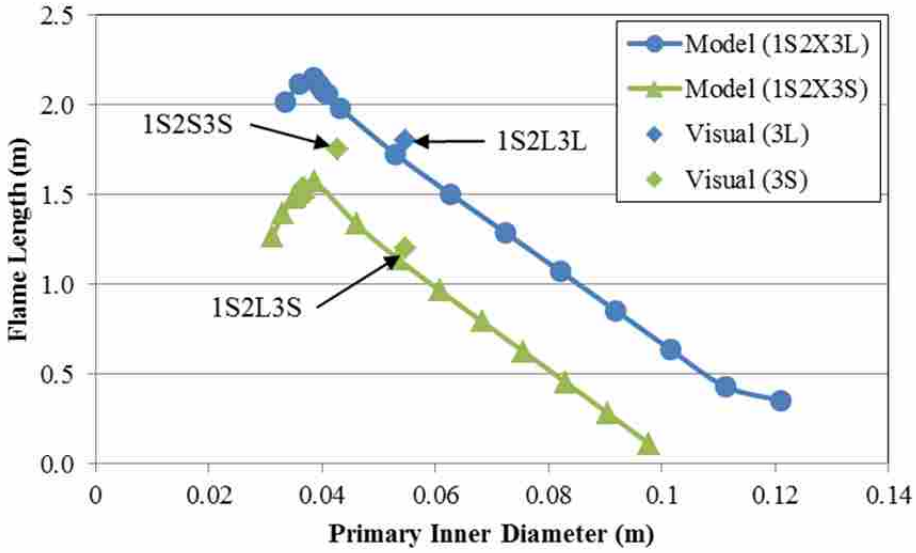

Figure 5.11: Visual or calculated flame length vs primary diameter for medium wood

The results show the flame length is longest at a primary diameter of 0.04m and decreases linearly with either smaller or larger primary diameter. The maximum occurs where the primary and secondary velocities are equal and there is no mixing due to shearing stresses between the two streams. The flame length is not infinite because there is still mixing caused by

recirculation as represented by the first term in the denominator of Equation 5.1. The triangle marked 1S2L3L shows the measured flame length for that burner (1S2L3L) which is in good agreement with the model.

The burner configuration with the smaller secondary diameter (3S) has shorter flame lengths because the area between the primary and secondary tubes is smaller creating a higher velocity for the secondary oxidizer and more swirl. Therefore the first term in the denominator of Equation 5.1 is larger. The same trend is apparent in the model where the flame is longest at a geometry which creates no velocity difference between the primary and secondary streams and the flame gets shorter as that velocity difference increases. The diamond marked 1S2L3S is shown to indicate the measured flame length which again agrees very well with the model. A third measured data point is shown where both the primary and secondary diameters are the smallest of the available hardware choices and this data point also agrees relatively well with the model as it should fall along with the triangular data points.

5.7.2 Secondary Diameter

The next variable investigated was the diameter of the secondary oxidizer tube (D_5, Figure 4.2). As secondary diameter increases with a fixed primary diameter, secondary area increases and secondary air velocity decreases reducing mixing between the two streams and increasing flame length. Figure 5.12 shows a trend of increasing flame length with increasing secondary diameter. As the secondary diameter increases from 0.07 to 0.24 m, the secondary air velocity is getting closer to the primary air velocity and therefore both first term (swirl mixing) and second term (shear flow mixing) in the denominator are getting smaller but the swirl controlled mixing term is dominant and therefore the flame length continues to grow with

increasing secondary diameter. Two measured data points are shown in the figure, which are in good agreement with both the magnitude and trend predicted by the model.

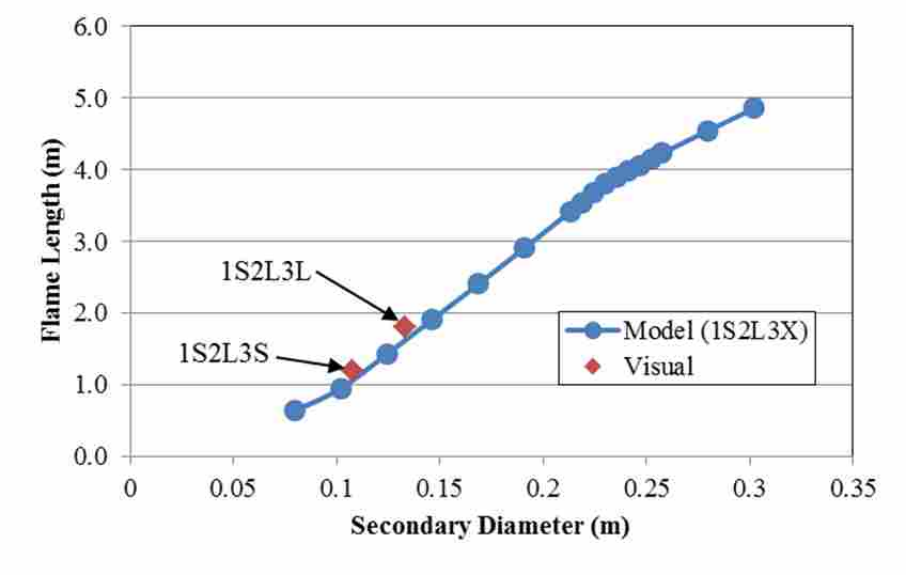

Figure 5.12: Visual or calculated flame length vs secondary diameter for medium wood

5.7.3 Primary Mass Flow

There are three ways to vary the primary mass flow: 1) Vary primary air flow, 2) vary fuel mass flow, and 3) vary total primary flow while holding the fuel to air ratio in the stream constant. Each of these is presented here.

Figure 5.13 shows the model predicts a slightly decreasing flame length with increasing primary air mass flow rate. The result is a combination of increased air to fuel ratio increasing favoring a shorter flame and increasing primary velocity to be closer to secondary flow velocity causing increased flame length. The net effect is a slightly shorter flame with increasing primary air flow rate.

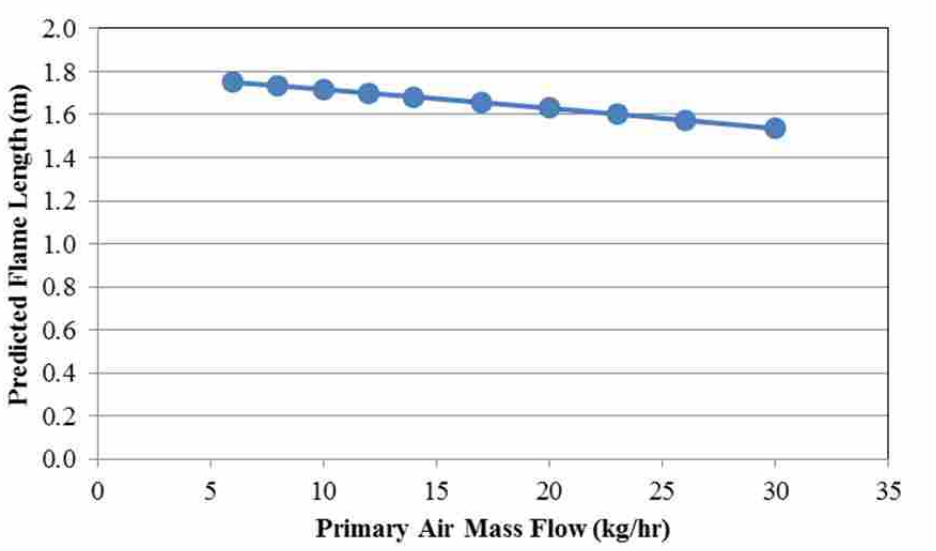

Figure 5.13: Predicted flame length vs primary air mass flow

Figure 5.14 shows a trend of increasing predicted flame length with increasing fuel flow rate. In this case adding fuel increases the fuel to oxidizer ratio causing longer flames while the fuel flow has little impact on the velocities and mixing rates between the primary and oxidizer streams.

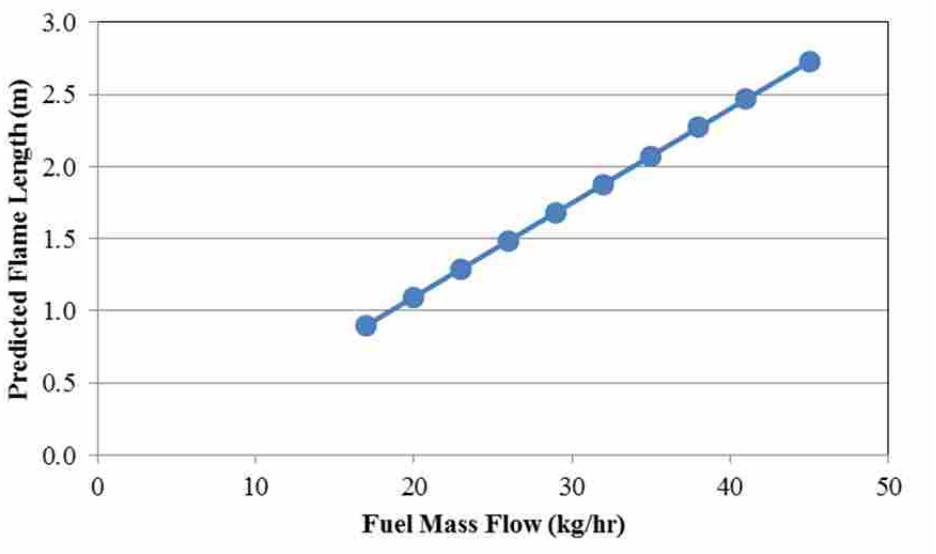

Figure 5.14: Predicted flame length vs fuel mass flow

Figure 5.15 shows a trend of an almost linear increase in flame length when both fuel and primary air flows increase in equal proportions. Equation 5.1 can be used to explain the trend. When the fuel air mixture in the primary is richer than stoichiometric, the first term in the numerator increases faster than the second term. Also, a higher mass flow rate means a higher primary velocity. As the primary velocity increases the difference between primary and secondary velocities decreases, causing reduced mixing between the two streams.

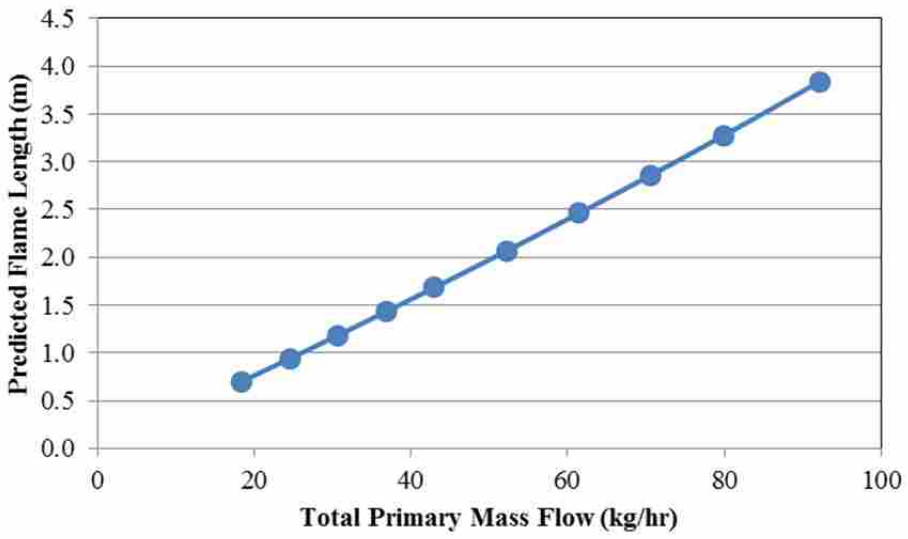

Figure 5.15: Predicted flame length vs total primary mass flow. Fuel-to-air ratio in primary stream is held constant

5.7.4 Secondary Air Mass Flow

Figure 5.16 shows a trend of decreasing flame length with increasing secondary air mass flow rate. Increasing secondary air flow increases shearing between secondary and primary flows and increases mixing by swirl, both of which reduce flame length. Experimental data for varying secondary air flow are shown in comparison to the model. There is good agreement in both magnitude and trend between the measured and predicted result.

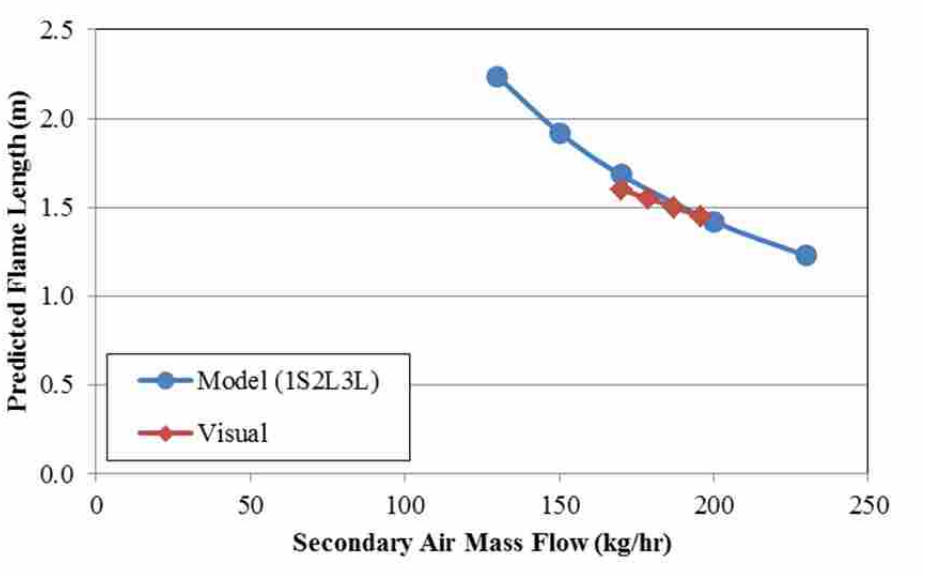

Figure 5.16: Measured and predicted flame length vs secondary air mass flow

5.7.5 Oxygen Enrichment

Oxygen was added in two locations: 1) Premixed with the secondary air or 2) Center injection. Figure 5.17 shows the trend produced by the model as the mass flow of enriching oxygen premixed into the secondary air varies. The model agrees with the measurements that there is a decrease in flame length with an increase in the amount of oxygen added to the secondary air. The model predicts both the absolute value and the change in flame length relatively well.

Figure 5.18 shows measured and modeled flame lengths with oxygen addition via the center tube. The model predicts a 33% drop in flame length with the addition of 8 kg/hr of oxygen. The data show a more moderate decrease on the order of 10%. The model assumes that all of the oxygen from the center tube is immediately mixed with the incoming fuel while the data suggest the oxygen takes time to mix and does not have as great an impact on flame length

as suggested by the model. This result was also found when comparing modeled and measured flame lengths for all other fuels.

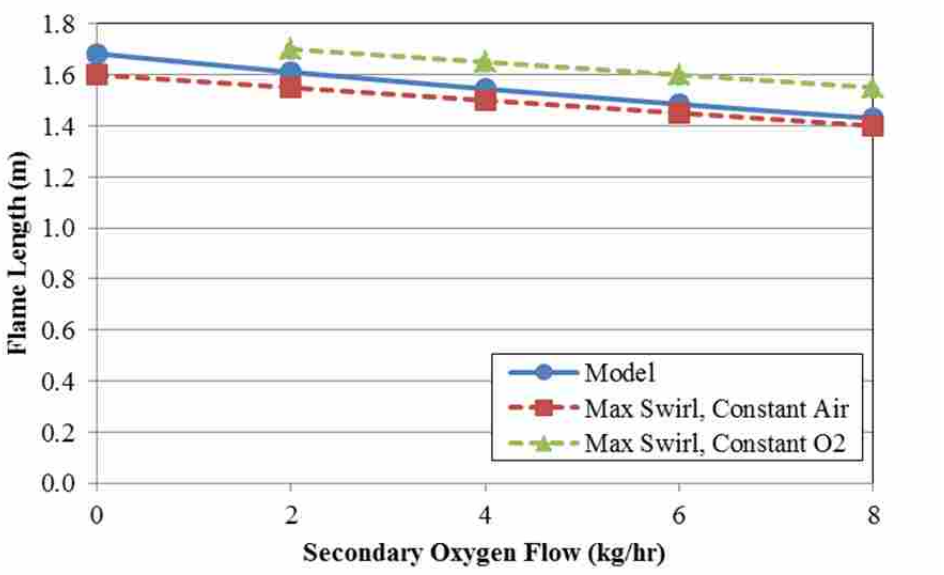

Figure 5.17: Measured and predicted flame length as a function of oxygen added to the secondary air.

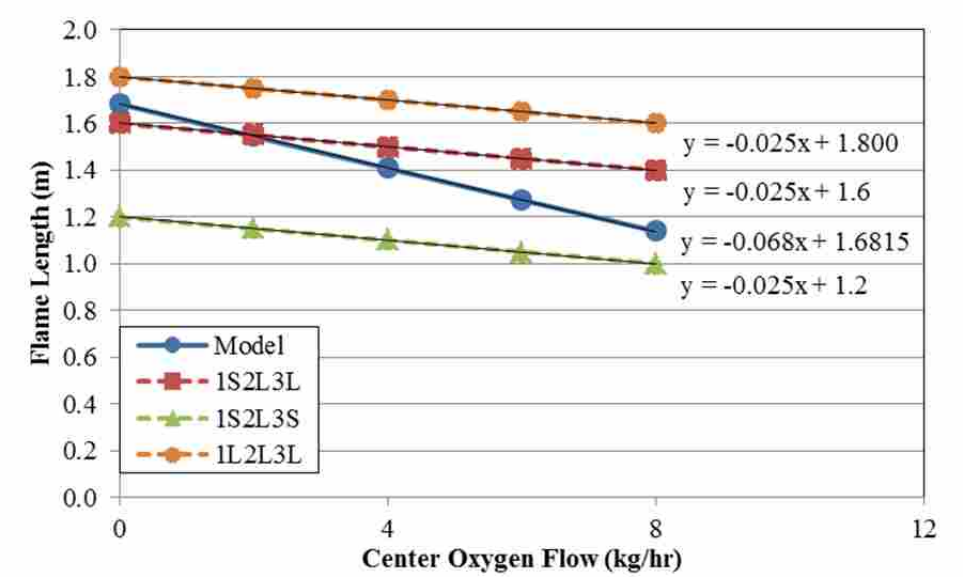

Figure 5.18: Flame length vs center oxygen mass flow

5.8 Predicting Empirical Constants

The model contains two empirical constants, c_1 and c_2, from a best fit for all of the data points for a given fuel and given reactor/burner combination. While this is useful for determining trends expected by changes in geometry, it was of interest to determine if a single set of constants could be used for all fuels and burner/reactor combinations or if the constant could somehow be determined without the need for experimental data. The values for c_1 and c_2 used in the results shown in Figure 5.10 are shown in Table 5.1. It was observed that for three of the five fuels, particularly those with smaller particles, c_1 is equal to zero suggesting mixing due to swirl is more important for these flames than mixing by shear. The data obtained for these flames did not include zero swirl and therefore a finite value for c_1 is needed to make the model more generally applicable.

Table 5.1: Values of empirical constants for each fuel

	c_1	c_2
Medium Wood	0.002851	0.021731
Straw	0	0.019396
Fine Wood	0	0.036819
Switchgrass	0.006844	0.012681
Coal	0	0.016059
U of U	0.00226	0.001947

Data taken in the oxyfuel combustor (OFC) at the University of Utah (U of U) without swirl produced a c_1 very close to the medium wood results in the BFR at BYU. Using this value (0.00226) for c_1 for all fuels new values for c_2 were determined for c_2 for each fuel as shown in Table 5.2. A comparison of measured and predicted flame lengths for all fuels using these values for c_2 are shown in Figure 5.19. The difference between these results and those in Figure 5.10 are

insignificant. The small impact of c_1 on the model is due to the fact that swirl is the dominant mode for mixing for most of the data obtained in this work.

Table 5.2: Values of empirical constants using the same c_1 for all fuels

	c_1	c_2
Medium Wood	0.00226	0.022488
Straw	0.00226	0.015871
Fine Wood	0.00226	0.033449
Switchgrass	0.00226	0.018762
Coal	0.00226	0.012807
U of U	0.00226	0.001947

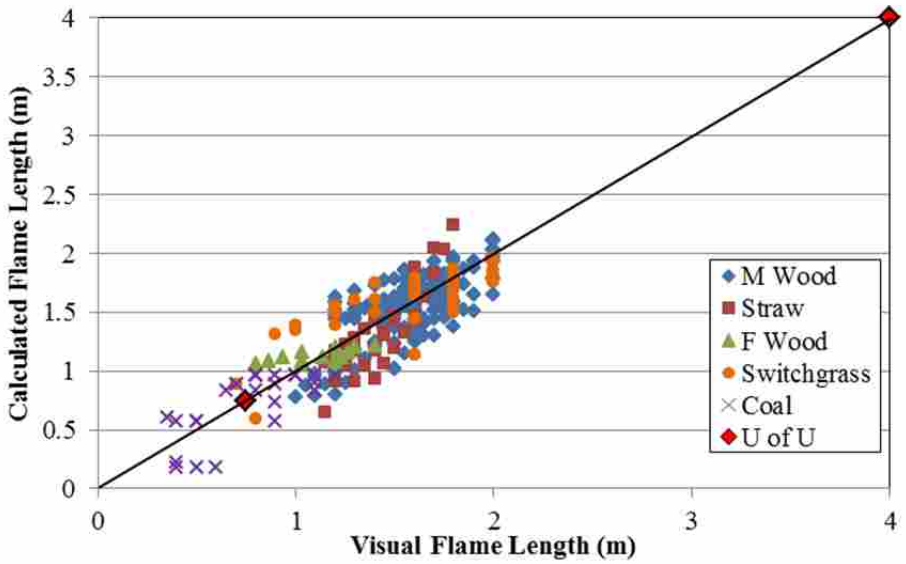

Figure 5.19: Calculated volatiles flame length vs visual volatiles flame length using a global constant c_1 for all fuels with unique c_2 for each fuel.

Values for c_2 are plotted as a function of fuel diameter in Figure 5.20. Early data seemed to suggest that c_2 was a function of particle diameter indicating that flames with small particles were more dependent on swirl induced mixing as the fine particles would follow the flow while

larger particles were more likely to penetrate a recirculation zone and mixing was controlled more by shearing between fuel and air flows. This correlation did not hold for all of the data and therefore an average value of $c_2 = 0.02$ was selected as the best option for predicting flame lengths when empirical data are not available.

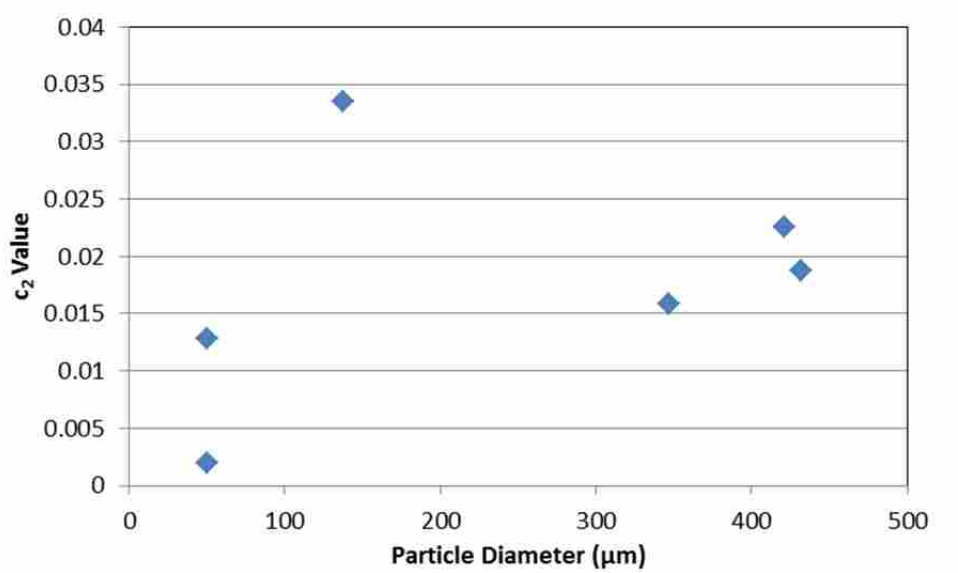

Figure 5.20: c_2 values vs average particle size for each fuel

Using c_1=0.00226 and c_2=0.02 for all fuels flame length was calculated and is compared to visual flame length in Figure 5.21. These data show fuels are clumped together but are overall more scattered than when the model constants can be determined by experimental results. The fine wood flames are all predicted to be longer than the measured flames and almost all of the straw flames are predicted to be shorter than the measured flames. The model predicted 90% of the flame lengths to be within 38% of the measured value.

Two types of data are not within 50% of the predicted flame length: coal flames in the BFR with center oxygen addition and the coal flame in the L1500. The reason for poor prediction of the BFR with center oxygen addition is discussed in Section 5.7.5 but involves the assumption that center oxygen addition is perfectly mixed at the burner exit.

The reason for a poor prediction of the L1500 flame length is not clear. This flame had significantly higher primary air to fuel ratio and higher velocities than the BFR burner. The physical size of the burner was only 50 – 100% larger than the BFR burner.

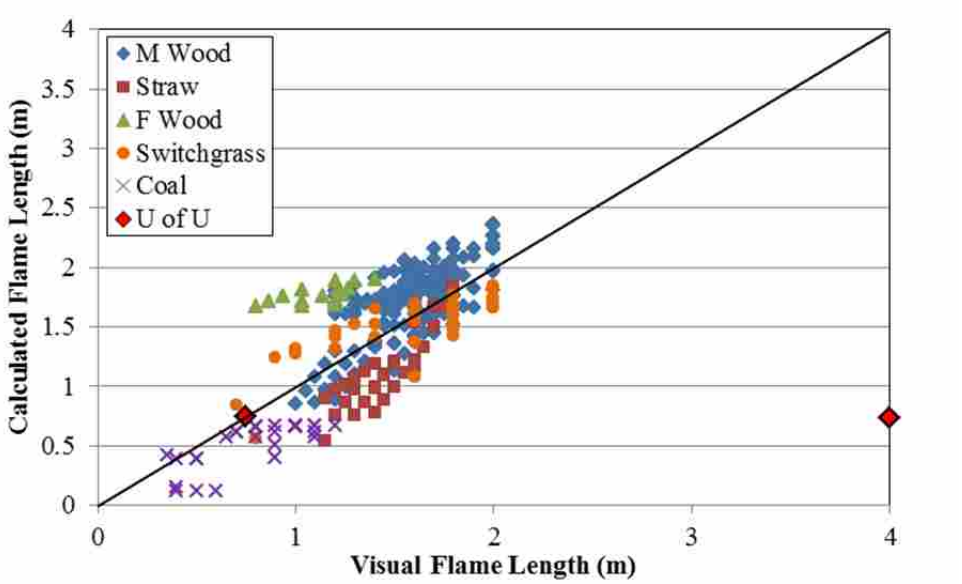

Figure 5.21: Calculated vs visual volatiles flame lengths with set values for both constants

5.9 Empirical Constants and the Stokes Number

A second method of predicting c_1 and c_2 explored in this work was to correlate their values with the Stokes number. In a study by Probstle and Wenz [32] the response of a particle to gas motion in a pulverized coal combustor was characterized by a "time constant" defined by Equation 5.2 where ρ_p is the density of the particle, d_p is the particle diameter, and μ_f is the dynamic viscosity of the fluid. A characteristic time of the fluid can be found as the ratio of a characteristic length of the fluid (l_f) to the fluid velocity (u_f) as shown in Equation 5.3. The ratio of the particle time constant, τ_p, and the fluid characteristic time, τ_f, creates Equation 5.4 which is often referred to as the Stokes number (Stk) and is a parameter that evaluates the tendency of a solid particle to follow the streamlines of the fluid flow or the inertial trajectory of the particle.

For Stk ≪ 1 the particle will follow the fluid flow streamlines and for Stk ≫ 1 the particle will follow its inertial trajectory.

$$\tau_p = \frac{\rho_p d_p^2}{18\mu_f} \tag{5.2}$$

$$\tau_f = \frac{l_f}{u_f} \tag{5.3}$$

$$Stk = \frac{\rho_p d_p^2 u_f}{18\mu_f l_f} \tag{5.4}$$

Using an average velocity of the primary stream (V_p) for u_f and the theoretical recirculation zone diameter (b) for l_f values for c_1 and c_2 were calculated for each fuel. Figure 5.22 and Figure 5.23 show these values and how they correlate with the Stokes number. c_1 appears to increase with increasing Stokes number while c_2 decreases with increasing Stokes number. However the trends in c_2 appear are offset for coal cases compared to biomass fuels. This is likely due to the amount of volatiles in the two types of fuels. Biomass fuels have higher volatile fractions which would require higher constants to acquire the correct flame length.

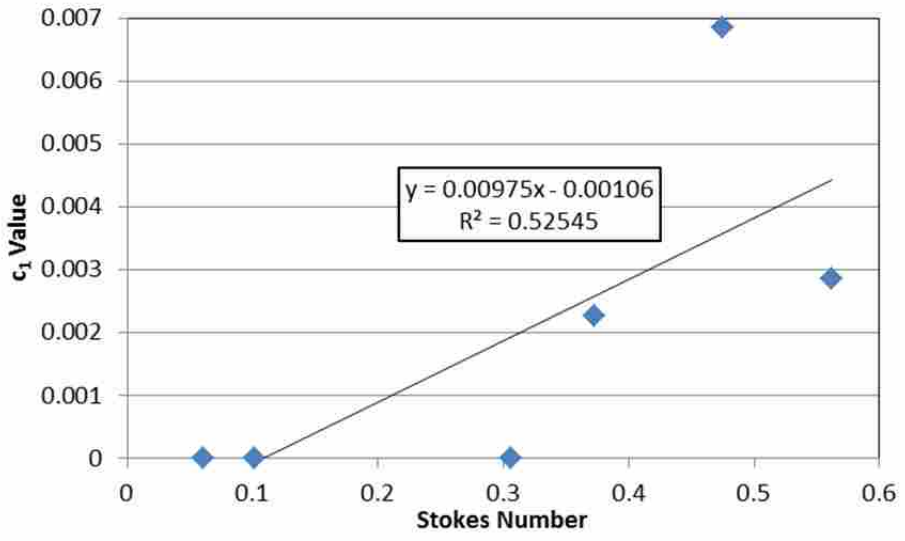

Figure 5.22: c_1 vs Stokes number for each fuel

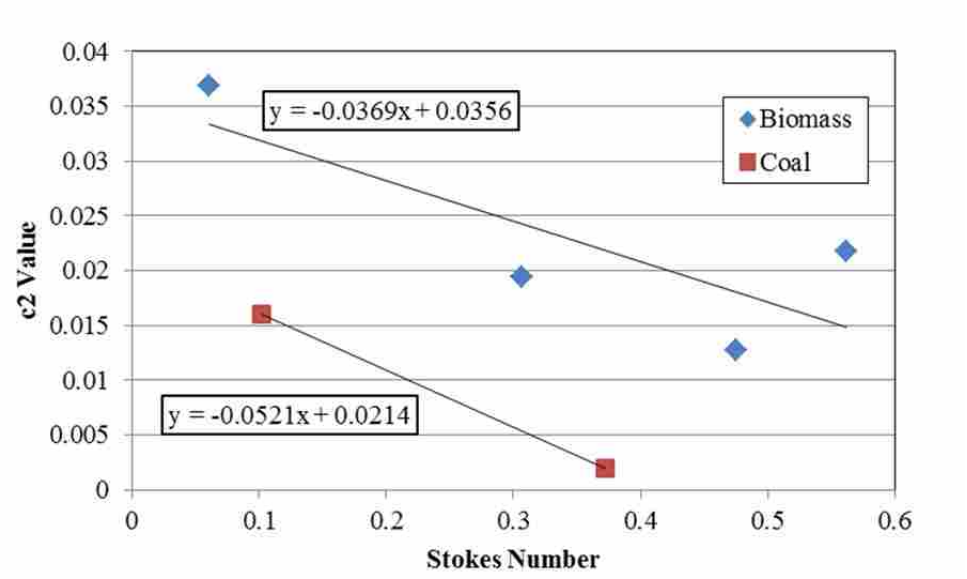

Figure 5.23: c_2 vs Stokes number for each fuel

Using the equations shown in these figures positive values for c_1 and c_2 were calculated and are shown in Table 5.3. The values of c_1 for fine wood and coal were slightly negative by the correlation but were set to zero. Using these values the model was once again compared to flame length data as shown in Figure 5.24. Using these predicted values for c_1 and c_2 based on the Stokes number of the particles, the model then predicted 90% of the flame lengths to be within 44% of the measured value.

Table 5.3: Values of c_1 and c_2 using the curve fit with Stokes number

	c_1	c_2
Medium Wood	0.004423	0.014851
Straw	0.001929	0.024288
Fine Wood	0	0.033371
Switchgrass	0.003574	0.018062
Coal	0	0.016099
U of U	0.002572	0.001993

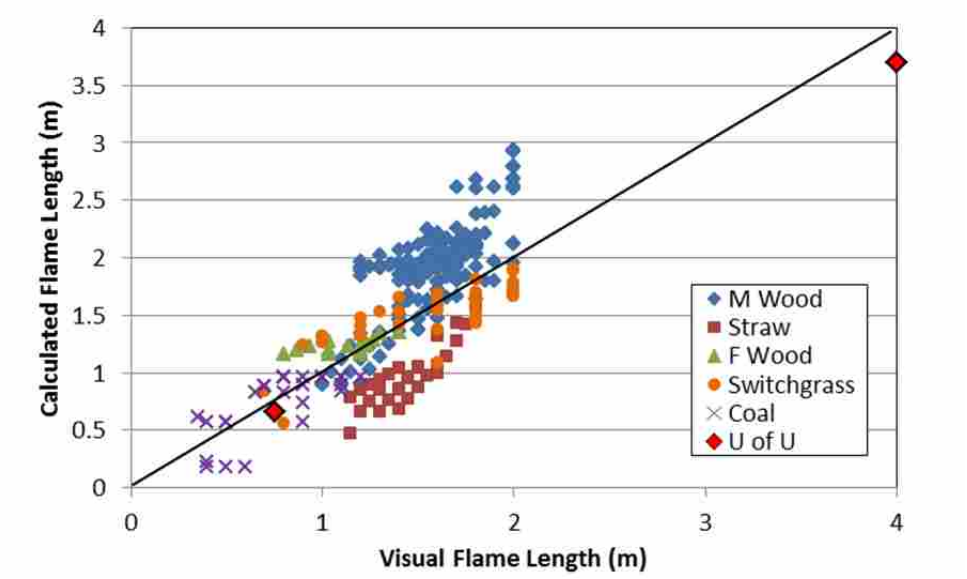

Figure 5.24: Calculated vs visual volatiles flame lengths with constants that are correlated with the Stokes number

5.10 Discussion

The agreement between measured and predicted flame lengths is surprisingly good for the wide range of conditions measured. The model is based on mixing considerations for gaseous flows and may capture effects related to particle trajectory when correlating c_1 and c_2 with the Stokes number, but still does not account for the effects of devolatilization time and particle heating rates. The data suggest that although these physical processes are important, fuel oxidizer mixing is the dominant factor in determining flame lengths for fine particle flames as it is in gaseous flames. Once a flame length has been established, the impact of a change in burner geometry on a change in flame length can be qualitatively assessed by considering the impact that change will have on mixing related to swirl and shearing. Oxygen addition directly into the fuel stream will have a greater impact on flame length than oxygen in an adjacent stream. When oxygen is added to a secondary stream, if the oxygen addition results in slower velocities and less mixing, the flame length will increase in spite of the added oxygen. Very long flames can

be obtained by matching fuel and oxidizer flow velocities and reducing swirl which limits mixing. This will also result in lifted unstable flames.

6 SUMMARY AND CONCLUSIONS

Experimental data were taken using a swirled burner with three coaxial tubes for nearly 400 operating conditions. Data for two new fuels, switchgrass and coal, which included about 100 data points, were added to the previous 300 BYU data points for hardwoods and straw from work done by Owen [3]. Data points consisted of varying swirl, fuel type, air flow rate, enhanced oxygen flow rate and oxygen addition location. Trends in NO and LOI were shown to correlate with flame length by Owen and data new to this work. Increasing flame length correlated with decreasing NO and increasing LOI. The analytical model developed by Owen [3] was compared to the current and previous flame length data.

The previous model did not predict changes in flame length when coal was used as the fuel. An improved model was proposed that included the ASTM volatile fraction as the amount of fuel entering the system instead of the total fuel mass flow. This improved the model's ability to predict trends in the length of coal flames while only changing the R^2 value of non-coal flames by less than 2%.

The model was used to explore trends involving the effect of burner geometries and mass flow rates on flame length. For each variable investigated, all other variables were held constant

1) Increasing primary tube diameter decreases flame length because the area of the secondary flow (annulus between primary and secondary tube) decreases increasing the secondary velocity and mixing between the two streams.
2) Increasing secondary tube diameter produces longer flames because the area of the secondary oxidizer is increased and the flow velocity decreases reducing mixing between fuel and oxidizer and decreasing swirl,
3) Increasing primary air flow produces shorter flames because oxidizer is added to the fuel stream.
4) Increasing fuel flow produces longer flames because more oxidizer mixing into the fuel stream is required to reach a stoichiometric mixture
5) Increasing secondary air flow produces shorter flames because it increases secondary oxidizer velocity and swirl increasing mixing between fuel and oxidizer.
6) Increasing oxygen flow in the secondary stream produces slightly shorter flames as the velocity is not greatly increased but the concentration of oxygen increases mixing of oxidizer into the fuel rich center.
7) Increasing oxygen flow in the center tube produces significantly shorter flames as the oxygen is added directly to the fuel rich center jet and decreases the oxygen required to mix the fuel to a stoichiometric mixture.

Two methods were investigated to determine constants that could be used with the model without additional empirical data. The first method looked at using a constant c_1 and c_2 for all fuels. The results showed that the model predicted 90% of the flame lengths within ±38% of the measured value.

The second method attempted to correlate c_1 and c_2 with the Stokes number. This technique allows the particle size to become a part of the flame length correlation. The c_1 results were found to correlate reasonably well with the Stokes number for all fuels while the c_2 data were correlated by the Stokes number within a given fuel type, coal or biomass. Biomass fuels have high volatile fractions and produced higher c_2 values than coal which is a lower volatile fuel. Using a single linear correlation for c_1 and separate linear correlations for c_2 for coal and biomass 90% of the predicted flame lengths were within 44% of the measured values.

REFERENCES

[1] C. A. T. Center, "Nitrogen Oxides (NOx), Why and How They Are Controlled," EPA, 1999.

[2] "Clean Air Act Overview," EPA, 30 March 2016. [Online]. Available: https://www.epa.gov/clean-air-act-overview/clean-air-act-text. [Accessed 11 November 2016].

[3] S. Owen, Burnout, NO, and Flame Characterization from an Oxygen-Enriched Biomass Flame, Provo: Brigham Young University, 2015.

[4] S. Azuhata, K. Narato, H. Kobayashi, N. Arashi, S. Morita and T. Masai, "A Study of Gas Composition Profiles for Low NOx Pulverized Coal Combustion and Burner Scale-up," in *Twenty-first Symposium (International) on Combustion/The Combustion Institute*, 1986.

[5] M. L. Holtmeyer, G. Li, B. M. Kumfer, S. Li and R. L. Axelbaum, "The Impact of Biomass Cofiring on Volatile Flame Length," *Energy & Fuels,* vol. 27, pp. 7762-7771, 2013.

[6] S. P. Burke and T. E. W. Schumann, "Diffusion Flames," *Industrial and Engineering Chemistry,* vol. 20, no. 10, pp. 998-1004, 1928.

[7] F. G. Roper, "The Prediction of Laminar Jet Diffusion Flame Sizes: Part I. Theoretical Model," *Combustion and Flame,* vol. 29, pp. 219-226, 1977.

[8] F. G. Roper, "The Prediction of Laminar Jet Diffusion Flame Sizes: Part II. Experimental Verification," *Combustion and Flame,* vol. 29, pp. 227-234, 1977.

[9] S. R. Turns, "Laminar Diffusion Flames," in *An Introduction to Combustion Concepts and Applications*, New York, McGraw Hill Education, 2014, pp. 311-365.

[10] J. A. Fay, "The Distributions of Concentration and Temperature in a Laminar Jet Diffusion Flame," *Journal of Aeronautical Sciences,* vol. 21, pp. 681-689, 1954.

[11] S. R. Turns, "Turbulent Nonpremixed Flames," in *An Introduction to Combustion Concepts and Applications*, New York, McGraw Hill Education, 2014, pp. 486-526.

[12] K. Wohl, C. Gazley and N. Kapp, "Diffusion Flames," in *Third Symposium on Combustion and Flame and Explosion Phenomena*, Baltimore, 1949.

[13] M. A. Delichatsios, "Transition from Momentum to Buoyancy-Controlled Turbulent Jet Diffusion Flames and Flame Height Relationships," *Combustion and Flame,* vol. 92, pp. 349-364, 1993.

[14] H. A. Becker and D. Liang, "Visible Length of Vertical Free Turbulent Diffusion Flames," *Combustion and Flame,* vol. 32, pp. 115-137, 1978.

[15] Y. Kang, T. Lu, X. Lu, X. Gou, X. Huang, S. Peng, X. Ji, Y. Zhou and Y. Song, "On Predicting the Length, Width, and Volume of the Jet Diffusion Flame," *Applied Thermal Engineering,* vol. 94, pp. 799-812, 2016.

[16] M. Hupa, "International Flame Research Foundation," 24 January 2006. [Online]. Available: http://www.ffrc.fi/Liekkipaiva_2006/Liekkipaiva2006_IFRF_Today_HUPA.pdf. [Accessed 10 November 2016].

[17] R.-H. Chen and J. F. Driscoll, "The Role of the Recirculation Vortex in Improving Fuel-Air Mixing within Swirling Flames," in *Twenty-Second Symposium (International) on Combustion/The Combustion Institue*, 1988.

[18] K. L. Smith, L. D. Smoot, T. H. Fletcher and R. J. Pugmire, "Devolatilization Rate Processes and Products," in *The Structure and Reaction Processes of Coal*, New York, Plenum Press, 1994, pp. 209-321.

[19] K. L. Smith, L. D. Smoot, T. H. Fletcher and R. J. Pugmire, "Char Oxidation, Conversion, and Reaction Rate Processes," in *The Structure and Reaction Processes of Coal*, New York, Plenum Press, 1994, pp. 325-404.

[20] K. L. Smith, L. D. Smoot, T. H. Fletcher and R. J. Pugmire, "Geochemistry and Macromolecular Structure of Coal," in *The Structure and Reaction Processes of Coal*, New York, Plenum Press, 1994, pp. 37-75.

[21] S. R. Turns, "Burning of Solids," in *An Introduction to Combustion Concepts and Applications*, New York, McGraw Hill Education, 2014, pp. 527-555.

[22] T. Chae, "Numerical simulations of a large scale oxy-coal burner," in *Cleaner Combustion and Sustainable World*, Springer-Verlag Berlin Heidelberg and Tsinghua University Press, 2012, pp. 643-645.

[23] L. Chen and A. F. Ghoniem, "Simulation of Oxy-Coal Combustion in a 100 kWth Test Facility Using RANS and LES: A Validation Study," *Energy & Fuels,* vol. 26, pp. 4783-4798, 2012.

[24] J.-D. Kim, G.-B. Kim, Y.-J. Chang, J.-H. Song and C.-H. Jeon, "Examination of Flame Length for Burning Pulverized Coal in Laminar Flow Reactor," *Journal of Mechanical Science and Technology,* vol. 24, no. 12, pp. 2567-2575, 2010.

[25] S. R. Turns, An Introduction to Combustion Concepts and Applications, New York: McGraw Hill Education, 2014.

[26] J. D. Thornock, "Burnout, NO, Flame Temperature, and Radiant Intensity from Oxygen-Enriched Combustion of a Hardwood Biomass," Brigham Young University, Provo, 2013.

[27] E. G. Eddings, "Institute for Clean and Secure Energy - Experimental Facilities," University of Utah, 2015. [Online]. Available: http://www.icse.utah.edu/experimental_facilities. [Accessed 13 March 2017].

[28] J. Zhang, K. Kelly, E. G. Eddings and J. Wendt, "OXY-coal combustion: Effects of PO2 on coal jet stability in O2/CO2 environments," *25th Annual International Pittsburgh Coal Conference, PCC - Proceedings,* 2008.

[29] A. Fry, Interviewee, *Personal Communication.* [Interview]. 9 August 2016.

[30] T. Fletcher, A. Kerstein, R. Pugmire, M. Solum and D. Grant, "A Chemical Percolation Model For Devolatilization: Summary," University of Utah, Salt Lake City.

[31] S. Niksa and A. Kerstein, "FLASHCHAIN Theory for Rapid Coal Devolatilization Kinetics. 1. Formulation," *Energy & Fuels,* no. 5, pp. 647-665, 1991.

[32] G. Probstle and W. Wenz, "Velocity Measurements in a Swirl Driven Pulverized Coal Combustion Chamber," *Combustion and Flame,* vol. 72, pp. 193-203, 1988.

APPENDIX A LOSS ON IGNITION (LOI) PROCEDURE

Loss on ignition was determined using the procedure outlined below. Small1.3 ml crucibles were used so that a minimal amount of ash would be required and so that three replications for each operating condition could be obtained from the ash collected.

1. Weigh empty ceramic crucibles (This weight will need to be subtracted from other weights measured in Steps 2, 4, and 6 for the actual weight of the ash)
2. Fill crucibles with ash to about ¾ maximum capacity to prevent spillage and weigh again
3. Heat sample in conventional oven at 105°C for 4 hours to remove moisture
4. Weigh crucibles for moisture free ash weight, W_{mfa}
5. Heat sample in conventional oven at 750°C for 6-8 hours
6. Weigh crucibles for carbon free ash, W_{cfa}
7. Calculate LOI using the following equation:

$$LOI = \frac{W_{mfa} - W_{cfa}}{W_{mfa}} \tag{A.1}$$

8. Carbon burnout may be calculated using the following equation where Y_{ash} is the ash content from ASTM proximate analysis

$$Carbon\ Burnout\ \% = \frac{1 - Y_{ash} - LOI}{(1 - LOI) * (1 - Y_{ash})} \tag{A.2}$$

APPENDIX B OXYGEN ENRICHMENT CONSTANT (C_3)

Figure 5.18 shows the trend produced by the model as the mass flow of enriching oxygen in the center tube varies. The model predicts a 33% drop in flame length with the addition of 8 kg/hr of oxygen. The data show a more moderate decrease on the order of 10%. The model assumes that all of the oxygen from the center tube is immediately mixed while the data suggest the oxygen remains more separate.

To correct the discrepancy a third constant was added to the model for the mass flow of oxygen in the center tube term so that the model becomes Equation B.1. This new constant was found by minimizing the error in the slope between experimental and visual flame lengths for each fuel. c_1 was held constant and c_2 was then curve fit to flame length data. All three constants for each fuel are listed in Table B.1.

$$L_f = \frac{\frac{\dot{m}_{fuel} f_v}{c_s} - \dot{m}_{O_2,p} - c_3 \dot{m}_{O_2,c}}{\left[\rho_{sec} \pi b U_{RZ} c_2 + \rho_{sec} \left|V_p - V_{sec}\right| d_p \pi c_1\right] Y_{O_2,sec}} \tag{B.1}$$

Table B.1: Values of all constants for each fuel

	c_1	c_2	c_3
Medium Wood	0.00226	0.023938	0.308109
Straw	0.00226	0.018225	0.221317
Fine Wood	0.00226	0.033448	1
Switchgrass	0.00226	0.018959	0.797446
Coal	0.00226	0.013123	0.778449

In Figure B.1 this refined version of the flame length model is compared to experimental data. The new constant appears to slightly reduce the overall error. Unfortunately there currently does not appear to be any physical explanation for this constant.

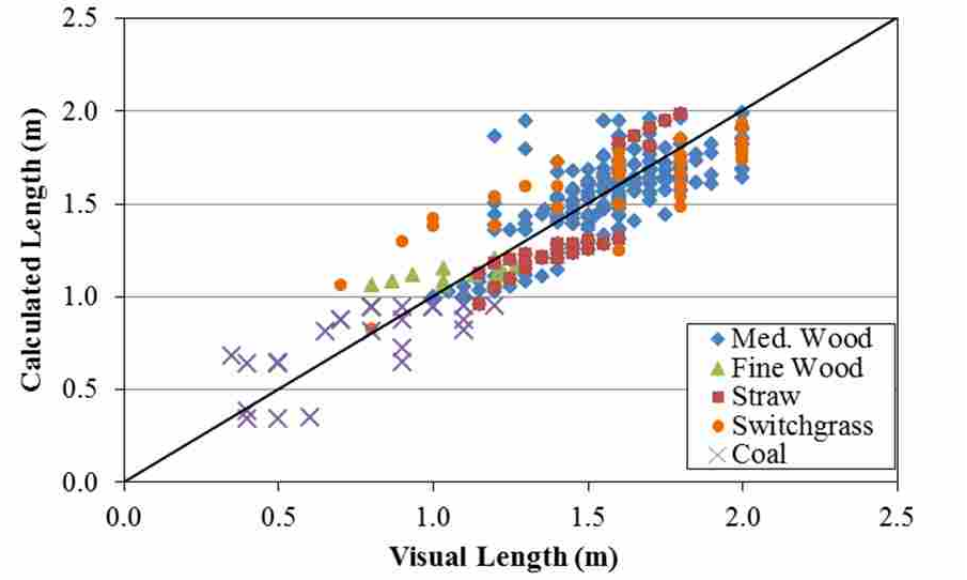

Figure B.1: Calculated flame length (m) with a third proportionality constant vs visual volatiles flame length